Electrochemical Energy Reviews (2022) 5: 4
https://doi.org/10.1007/s41918-022-00139-5

REVIEW ARTICLE

Copper-Based Catalysts for Electrochemical Carbon Dioxide Reduction to Multicarbon Products

Fangfang Chang[1] · Meiling Xiao[2] · Ruifang Miao[1] · Yongpeng Liu[1] · Mengyun Ren[1] · Zhichao Jia[1] · Dandan Han[1] · Yang Yuan[1] · Zhengyu Bai[1] · Lin Yang[1]

Received: 5 February 2021 / Revised: 23 August 2021 / Accepted: 8 November 2021 / Published online: 2 August 2022

Abstract
Electrochemical conversion of carbon dioxide into fuel and chemicals with added value represents an appealing approach to reduce the greenhouse effect and realize a carbon-neutral cycle, which has great potential in mitigating global warming and effectively storing renewable energy. The electrochemical CO_2 reduction reaction (CO_2RR) usually involves multiproton coupling and multielectron transfer in aqueous electrolytes to form multicarbon products (C_{2+} products), but it competes with the hydrogen evolution reaction (HER), which results in intrinsically sluggish kinetics and a complex reaction mechanism and places higher requirements on the design of catalysts. In this review, the advantages of electrochemical CO_2 reduction are briefly introduced, and then, different categories of Cu-based catalysts, including monometallic Cu catalysts, bimetallic catalysts, metal-organic frameworks (MOFs) along with MOF-derived catalysts and other catalysts, are summarized in terms of their synthesis method and conversion of CO_2 to C_{2+} products in aqueous solution. The catalytic mechanisms of these catalysts are subsequently discussed for rational design of more efficient catalysts. In response to the mechanisms, several material strategies to enhance the catalytic behaviors are proposed, including surface facet engineering, interface engineering, utilization of strong metal-support interactions and surface modification. Based on the above strategies, challenges and prospects are proposed for the future development of CO_2RR catalysts for industrial applications.

Keywords C_2 products · Carbon dioxide · Nanocatalysts · Electrochemical reduction · Mechanism

1 Introduction

In the past century, the concentration of carbon dioxide in the atmosphere has been dramatically increased due to the excessive burning of fossil fuels. CO_2 emissions continue to steadily grow from 280 ppm (1 ppm = 1×10^{-6}) before the industrial revolution to 419 ppm in 2019 and lead to serious environmental problems that threaten human's sustainable development [1–4]. In this context, intensive research efforts have been devoted to reducing CO_2 emissions and exploring new technologies for the separation, capture and conversion of CO_2 via electrocatalysis, photocatalysis and biological hybrids [5–13]. Among them, electrochemical reduction of CO_2 has attracted more attention in recent years due to its advantages of a simple system structure, mild reaction conditions, easy modularization and controllable conversion scale [14]. In the electrochemical CO_2 reduction process, carbon dioxide molecules and water molecules can be converted into valuable compounds (e.g., carbon monoxide, formic acid, methane, methanol, ethanol, ethylene and glycol ethylene) by using electricity generated by renewable energy (wind energy, solar energy and tidal energy). Such a process can realize efficient storage of electric energy and reduction of carbon dioxide emission, which has broad application prospects [15–19].

CO_2 is a linear central symmetric molecule and has two C=O bonds with a 116.3 pm bond length, which is shorter than those of C–O bonds and other multibond

✉ Zhengyu Bai
baizhengyu@htu.edu.cn

✉ Lin Yang
yanglin@htu.edu.cn

[1] Collaborative Innovation Center of Henan Province for Green Manufacturing of Fine Chemicals, Key Laboratory of Green Chemical Media and Reactions, Ministry of Education, School of Chemistry and Chemical Engineering, Henan Normal University, Xinxiang 453007, Henan, China

[2] Department of Chemical Engineering, University of Waterloo, Waterloo, ON N2L 3G1, Canada

functional groups [20]. Therefore, the bond energies are higher in the CO_2 molecule, and higher energy (approximately 800 kJ mol^{-1}) than for other carbonyl groups is required to dissociate the C=O bond. As a result, CO_2 molecules are very stable and react with H_2O molecules only under severe conditions (high temperature, high pressure and high potential) [21, 22]. The electrochemical CO_2 reduction reaction (CO_2RR) involves multiple proton-coupled electron transfer steps ($2e^-$, $4e^-$, $6e^-$ and $8e^-$) to yield a series of products, leading to slow reaction kinetics and a complicated reaction mechanism. In addition, electrocatalytic reduction of CO_2 in aqueous solution usually competes with the hydrogen evolution reaction (HER), which causes decreased energy efficiency [23–25].

Due to the complexity of the final products for the CO_2RR, the single-chamber electrolytic cell cannot meet the requirements. The CO_2RR in aqueous solution is usually performed in a three-electrode system of an H-type electrolytic cell. As shown in Fig. 1, the typical cell includes a working electrode, a counter electrode, a reference electrode and an ion exchange membrane to separate the cathode and anode reactions. Notably, the working electrode and the reference electrode are in the cathode cell, whereas the counter electrode is in the anode cell. The CO_2RR occurs at the cathode, and the oxygen evolution reaction (OER) occurs at the anode. Carbon dioxide gas is bubbled into the cathode cell, and the gas product directly enters into the gas chromatograph. The electrolyte contains positive and negative charges to promote the transport of CO_2 to the surface of the electrocatalyst and affect the energy barrier of CO_2 reduction. The ion exchange membrane separates the oxidation and reduction products and transfers protons to the cathode while maintaining charge balance. This device is simple and easy to operate with excellent gas tightness and good controllability, which is suitable for studying the intrinsic characteristics of catalysts [20].

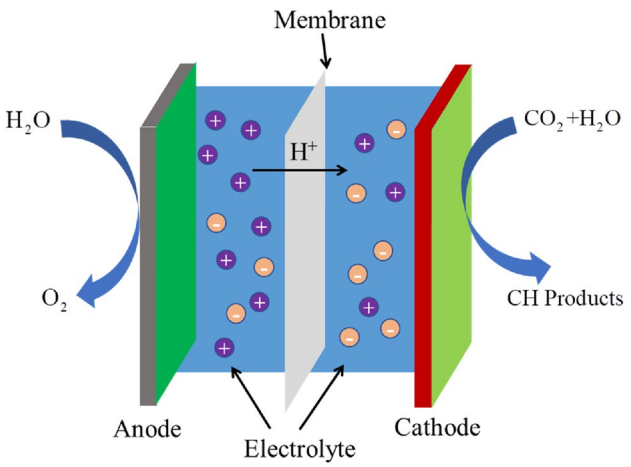

Fig. 1 Typical electrochemical CO_2RR system

The CO_2RR usually involves three steps at the interface between the catalyst surface and the electrolyte: (i) CO_2 molecules adsorb on the catalyst surface; (ii) intermediate products are reduced to form C–O, C–H or C–C bonds; and (iii) the new intermediates are recombined and then desorb from the electrode surface to form the product and diffuse into the electrolyte. The CO_2RR operates under mild reaction conditions and converts CO_2 into value-added fuels without high temperature and high pressure.

Important Parameters of the CO_2RR Metal atoms (or ions) are the active centers for most of the CO_2RR. During the reduction process, CO_2 adsorbs on the active center by taking advantage of the weak electrophilicity of CO_2 molecules and is then reduced by electrons from the cathode (usually accompanied by proton coupling), inducing the C=O bond to open and forming the C–H bond or C–C bond. For the CO_2RR, performance optimization should be considered mainly from the aspects of the following parameters.

(1) Onset potential

The onset potential is the potential applied between the working electrode and the reference electrode that is required to drive the CO_2RR. In general, the voltage at the transition junction between the thermodynamic control region and the kinetic control region is defined as the onset potential, which is usually lower than the equilibrium potential of the CO_2RR [26].

(2) Current density (j)

The current density represents the number of transferred electrons passing through the electrolyte and electrode barrier per unit area per unit time, which reflects the kinetic rate of electrochemical transformation [27]. The current density is normalized to the mass or surface area of the catalyst and is an essential indicator of the reaction rate on a specific electrocatalyst. For the CO_2RR, the overall current density is usually calculated by dividing the current by the geometric surface area of the working electrode. Therefore, the current density can be significantly increased by using nanostructured electrode materials with a large actual surface area while keeping the geometric area constant.

(3) Overpotential (η)

The overpotential is the difference between the actual potential of the reaction and the thermodynamic equilibrium potential, which reflects the efficiency of the conversion of electrical energy to chemical energy during electrolysis. The rapid consumption of substrate molecules near the electrode and the activation of the catalyst result in an overpotential [28]. The overpotential is closely related to the current density. The substrate molecules are consumed more rapidly on the electrode surface as the current density increases, and then, the reaction kinetics become more restricted to the diffusion

process, which leads to an increase in the overpotential. The overpotential is an important parameter to evaluate the catalytic performance of electrocatalysts and is susceptible to environmental factors (solvent, temperature and electrolyte pH).

(4) Faradaic efficiency for specific products (FE)

The Faradaic efficiency (FE) for a certain product is the percentage of electrons consumed to produce the specific product, which reflects the selectivity for the specific product [29, 30]. The FE for a specific product is calculated using the following equation:

$$\mathrm{FE} = \frac{\alpha n F}{j\left(\mathrm{mA\,cm^{-2}}\right) \times t(\mathrm{s})} = \frac{\alpha n F}{Q}$$

where α is the transferred electron number (e.g., $\alpha = 2$ is the electron number for electrochemical reduction from CO_2 to CO), n refers to the mole number of a given product, F is Faraday's constant (96 500 C mol^{-1}), Q is the amount of charge for a specific reaction (C), and j is calculated to normalize the FE to the amount of catalysts or electrochemically active surface area; the FE is the key indicator of the specific electrocatalyst reaction rate. A high FE (> 80%) for the specific product is one of the most important requirements for an ideal CO_2RR electrocatalyst.

(5) Tafel slope

The Tafel slope is an important parameter to evaluate the performance of electrocatalysts. According to the Butler-Volmer equation, Tafel plots can correlate the overpotential of the reduction reaction with the current density, and the equation is as follows:

$$\eta = \left(\frac{-2.3RT}{\alpha n F}\log j^0\right) + \left(\frac{2.3RT}{\alpha n F}\log j\right) = \alpha + b\log j$$

where j^0 is the exchange current density, α is the mass transfer coefficient, n is the number of transferred electrons, F is Faraday's constant, R is the gas constant (8.314 J K^{-1} mol^{-1}), and T is the thermodynamic temperature. The Tafel slope is determined based on the specific product and is an analytical indicator to reflect the rate-determining process.

(6) Energy efficiency (EE)

The energy efficiency (EE) is defined as the total energy utilization for the required product. The equation is as follows:

$$\varepsilon_{\mathrm{energetic}} = \frac{E_{\mathrm{eq}}}{E_{\mathrm{eq}+\eta}} \times \varepsilon_{\mathrm{Faradaic}}$$

where E_{eq} is the equilibrium potential and η is the overpotential. A high EE of CO_2 reduction is based on a low overpotential and a high FE.

(7) Stability

In addition to activity and selectivity, stability is another important parameter to evaluate an electrocatalyst for its practical application. Stability is usually evaluated by cyclic voltammetry (CV), chronoamperometry (CA) or chronopotentiometry (CP). The study of the stability of electrocatalysts and the understanding of their degradation mechanisms are beneficial for further optimization of electrocatalysts.

The CO_2RR usually involves multiproton coupling and multielectron transfer in aqueous electrolytes, varying from $2e^-$ to $18e^-$ to form different products C_1 (CO, HCOOH, HCHO, CH_3OH and CH_4) and C_2 (CH_3COOH, C_2H_4 and CH_3CH_2OH) [31, 32]. Table 1 summarizes the CO_2RR products of some chemical reactions.

During the CO_2RR process, there is a relatively high energy barrier to initiate the CO_2RR. Therefore, appropriate electrocatalysts should be selected to reduce the reaction energy barrier and improve the catalytic activity and product selectivity. On the catalysts, the CO_2RR proceeds via three elemental steps: first, CO_2 adsorbs on the metal electrode in

Table 1 Standard potentials for electrochemical reduction of CO_2

Reaction pathways	Potential (vs. SHE)/ V[a]
$CO_2(g) + 4H^+ + 4e^- \rightarrow C(s) + 2H_2O(l)$	0.210
$CO_2(g) + 2H_2O(l) + 4e^- \rightarrow C(s) + 4OH^-$	−0.627
$CO_2(g) + 2H^+ + 2e^- \rightarrow HCOOH(l)$	−0.250
$CO_2(g) + H_2O(1) + 2e^- \rightarrow HCOO^-(aq) + OH^-$	−1.028
$CO_2(g) + 2H^+ + 2e^- \rightarrow CO(g) + H_2O(l)$	−0.106
$CO_2(g) + H_2O(l) + 2e^- \rightarrow CO(g) + 2OH^-$	−0.934
$CO_2(g) + 4H^+ + 4e^- \rightarrow CH_2O(l) + H_2O$	−0.070
$CO_2(g) + 3H_2O(l) + 4e^- \rightarrow CH_2O + 4OH^-$	−0.898
$CO_2(g) + 6H^+ + 6e^- \rightarrow CH_3OH(l) + H_2O$	0.016
$CO_2(g) + 5H_2O(l) + 6e^- \rightarrow CH_3OH(l) + 6OH^-$	−0.812
$CO_2(g) + 8H^+ + 8e^- \rightarrow CH_4(g) + 2H_2O$	0.169
$CO_2(g) + 6H_2O(l) + 8e^- \rightarrow CH_4(g) + 8OH^-$	−0.659
$2CO_2(g) + 2H^+ + 2e^- \rightarrow H_2C_2O_4(aq)$	−0.500
$2CO_2(g) + 2e^- \rightarrow C_2O_4^{2-}(aq)$	−0.590
$2CO_2(g) + 12H^+ + 12e^- \rightarrow CH_2CH_2(g) + 4H_2O$	0.064
$2CO_2(g) + 8H_2O(1) + 12e^- \rightarrow CH_2CH_2(g) + 12OH^-$	−0.764
$2CO_2(g) + 12H^+ + 12e^- \rightarrow CH_3CH_2OH(l) + 3H_2O(l)$	0.084
$2CO_2(g) + 9H_2O(1) + 12e^- \rightarrow CH_3CH_2OH(l) + 12OH^-$	−0.744

[a]Equilibrium potential at 25 °C and 100 kPa, proton activity of 1 mol L^{-1}

aqueous solution; subsequently, an electron transfers to CO_2 to generate a $*CO_2^-$ intermediate, which is considered the decisive step of the reaction [31, 32]; and finally, $*CO_2^-$ is further reduced to the final product. Electrocatalysts for CO_2 reduction can be divided into the categories of metal catalysts, nonmetal catalysts and molecular catalysts, among which metal nanocatalysts have attracted particular attention due to their novel physical and chemical properties [33]. In addition, a high catalytic surface area and more active sites with edges and corners or low coordination endow metal nanocatalysts with completely different catalytic behaviors than flat surfaces and bulk metals with complete coordination [34, 35]. In 1985, Hori et al. systematically studied the performance of multiple metal electrodes for the CO_2RR [36–39]. After analyzing the products, these metals could be divided into four categories based on the different reduction products. (i) Metals such as Pt, Ni, Fe and Co, which had low hydrogen-producing overpotential and strong adsorption of carbon monoxide intermediates. The strong affinity of CO hindered the removal of intermediates and thus resulted in the inaccessibility of active sites for CO_2 adsorption. As a result, these metals were more suitable for the HER (e.g., Pt was a very good catalyst for the HER) compared with transition metal catalysts. (ii) Sn, Pb, Bi, In and other metal electrodes, on which the main product was formate with a small amount of CO and CH_4. This occurred because the $CO_2^{\cdot-}$ intermediate was difficult to adsorb but easily protonated after desorption and converted into formic acid or formate on these metals. (iii) Au, Ag, Zn, etc., which could catalyze CO_2 reduction to produce CO and a small amount of formic acid. These metals could adsorb the $CO_2^{\cdot-}$ intermediate and break the C–O bond to form carbon monoxide, which could easily desorb from the electrode surface as the main product. (iv) Copper, which was the only metal element that could generate C_1–C_3 hydrocarbon products due to its moderate adsorption energy for carbon monoxide. Carbon monoxide adsorbed on the electrode surface was hydrogenated to form a COH or CHO intermediate, and a C–C bond was further formed to obtain C_{2+} products. The products of Cu electrodes mainly included methane, formic acid and hydrogen, in addition to a small amount of CO. Beyond that, a C_2 product (e.g., ethylene) with an FE up to 20% at 40 °C was also detected on the surface of Cu electrodes [37]. Then, C_2 (e.g., C_2H_5OH) and C_3 (C_3H_7OH) products were further confirmed to be detected on Cu electrodes [38, 39]. Reduction products were also detected on the surface of Cu catalysts for the CO_2RR (electrolyte solution: 0.1 mol L^{-1} $KHCO_3$, voltage range: from −0.7 to −1.2 V versus reversible hydrogen electrode (RHE)), in which there were four C_1 products, seven C_2 products and five C_3 products [40]. The reasons for the differences in the products of carbon dioxide reduction catalyzed by metal catalysts have been systematically researched [41]. The CO_2RR involves multiple steps that occur on the surface of metal catalysts. The absorption of carbon dioxide intermediates on metal catalysts (adsorbed on the surface) is a key factor that determines the type of catalytic products. Au, Ag, Zn and other transition metals have weak absorption of carbon dioxide intermediates, and the catalytic reaction has a high initial potential. Generally, after adsorption and activation of carbon dioxide on the surface of metal catalysts, only one C=O bond can be broken to form CO and then release the products after desorption of the intermediate. The CO_2RR on Cu catalysts is more complex, on which the absorption of the CO_2RR intermediate is neither too strong nor too weak. In addition, Cu catalysts can break the C=O bond and produce hydrocarbons or even ethanol and propylene. These C_2 products as raw materials for many industrial production processes are more valuable than HCOOH and CO. However, due to the complexity and difficulty of multielectron reactions, the amount of ethanol and propylene in the products was relatively low [42], and designing Cu-based catalysts with high selectivity and activity for the electroreduction of CO_2 is very important. In this review, we focus on Cu-based catalysts in terms of their synthesis method and the conversion of CO_2 to C_{2+} products, the possible reaction mechanism, and the material strategies toward designing catalysts with improved selectivity for the reaction to C_{2+} products.

2 Representative Catalysts and Synthesis Methods

The CO_2RR is one of the most powerful means of artificial photosynthesis. During the electrocatalytic reduction process, an external bias is applied to the electrocatalysts for electroreduction of carbon dioxide molecules that adsorb on the surface of catalysts to value-added products (C_2H_4, C_2H_5OH, etc.). In general, electrocatalysts for the CO_2RR reported include the following categories: monometallic Cu catalysts, bimetallic Cu-based catalysts, metal–organic frameworks (MOFs) along with MOF-derived catalysts and other catalysts, which can convert CO_2 to C_{2+} products.

2.1 Monometallic Cu Nanocatalysts

In the past few decades, metal catalysts (e.g., Au, Ag, Sn and Cu) have been extensively studied for the electrocatalytic reduction of carbon dioxide [43–46]. The empty d orbital in the metal element can coordinate with CO_2 in the electrochemical reaction to reduce the energy of the C=O bond, thus catalyzing the CO_2RR. In most cases, the formation of CO_2 reactive intermediates is considered to be the rate-determining step in the CO_2 reduction process. Therefore, one of the most important functions of electrocatalysts is to stabilize the intermediates to achieve high reaction efficiency. The surface of a transition metal is more complex in the CO_2RR process. Although bulk metals exhibit good catalytic activity

for electrochemical CO_2 reduction, they are susceptible to poisoning and deactivation due to their low specific surface area. Metal nanocatalysts with a high specific surface area, abundant active sites and low ligand sites are more appealing and have shown great application potential in the electrochemical reduction of CO_2. Copper, as the only metal for the CO_2RR to C_2 and multicarbon products (C_2H_4, C_2H_5OH, CH_3COO^-, n-C_3H_7OH, etc.), has been extensively studied.

At present, numerous monometallic Cu catalysts with various morphologies/nanostructures have been reported, including Cu nanoparticles (Cu NPs) [47], Cu nanowires (Cu NWs) [48, 49] and three-dimensional (3D) Cu foam [42, 50], on which the catalytic performance highly depends on their surface properties. For the preparation of Cu NPs, the solvothermal method is commonly used. In the work conducted by Strasser's group, a monodispersed Cu NP catalyst with controllable size was prepared by reverse micelle encapsulation. The poly(styrene)-block-poly(2-vinylpyridine) (PS-P2VP) diblock copolymer with polar head (PVP) and nonpolar tail (PS) blocks was dissolved in nonpolar toluene to form reverse micelles, and the size of the NPs could be well tuned by adjusting the metal salt/PVP ratio or the molecular weight of the PVP head [51]. Uniform Cu NPs with sizes ranging from 2 to 15 nm were systematically investigated, and the results showed that the overall current density of the CO_2RR on the Cu NP catalyst displayed a sharp enhancement compared with that on bulk Cu electrodes, especially for Cu NPs below 5 nm. The main reaction products were hydrogen, carbon monoxide, methane and ethylene. The selectivity for specific products in the CO_2RR was found to be highly correlated with the size of the NPs, and the formation of hydrocarbons (methane and ethylene) was inhibited on the Cu NPs, particularly for NPs below 5 nm; HER was the dominant reaction, and the FE reached over 60%. Although Cu NPs are more selective for the CO product, the FEs for CO_2 reduction are generally lower. Larger Cu NPs of 40–60 nm were examined, and the ratio of the FEs for ethylene to methane was found to be 51.2 [52]. Cu nanospheres and nanocubes (Cu NCs) with different sizes (7.5 nm and 27 nm for Cu nanospheres and 24 nm, 44 nm and 63 nm for Cu NCs) were synthesized by using the same colloidal chemistry method. Their performance comparison for the CO_2RR revealed that the activity increased with decreasing NP size in the same morphology. However, the large-size Cu NCs (44 nm) had a higher performance in ethylene production than the small-size Cu nanospheres (27 nm). The FE for ethylene on Cu NCs reached 41%, twice that for methane [53]. Using the solvothermal method and tetradecyl phosphonic acid as a surface ligand, Cu NPs with a size of 6.7 nm were synthesized by reducing copper precursors at high temperature [54]. Scanning electron microscopy (SEM) images showed that monodispersed Cu NPs were loaded onto carbon paper with different loading densities, which systematically increased from the lowest loading of Cu × 1 loading (2 μg) to × 5 loading (10 μg) and × 22.5 loading (45 μg). Cu NPs were mostly independent and dispersed at the lowest loading and were closely arranged when the loading was increased to 22.5 times, as shown in Fig. 2a. Figures 2b–2d show that the FEs for the C_2 and C_3 products were significantly increased with increasing loading density, while the FE for the C_1 products was decreased, which was due to the improved carbon-carbon coupling reaction induced by reducing the distance between Cu NPs. Meanwhile, H_2 was found to be the main product in the first few minutes for the high-loading Cu catalysts. As the reaction proceeded, the FE for ethylene increased, and ethylene was the dominant product. After the reaction, the surface of the electrode was examined by SEM. The SEM images showed that the size of Cu NPs increased from 6.7 nm to larger cube-like NPs (10–40 nm), which occurred at the surface of the electrode in situ in a few minutes. The selectivity of Cu NPs with different particle densities was also studied for the CO_2RR, and the results revealed that the FE for ethylene compared with methane increased with increasing particle density [55]. At a high density of Cu NPs, CO obtained by initial reduction readsorbed on the surface of the catalyst and then drove the reaction of carbon-carbon coupling to obtain C_2 products. The electropolishing method could be used to pretreat Cu NPs with different catalyst surfaces. Cu NPs were pretreated by an electropolishing method to prepare copper electrodes with rough polycrystalline and sprayed NPs [56]. Rough polycrystalline Cu NPs or sprayed NPs were studied for the CO_2RR and showed excellent electrocatalytic performance for electrocatalytic reduction of carbon dioxide compared with copper electrodes with smooth surfaces because the rough Cu electrodes had higher specific surface area to provide more active sites and increase the current density during the electrochemical CO_2RR. Moreover, the copper electrodes with a rough surface had a higher selectivity for hydrocarbon products in the CO_2RR process, indicating that surfaces with different morphologies play an important role in the electrocatalytic reduction of carbon dioxide. Compared with nanocatalysts with smooth surfaces, nanocatalysts with rough surfaces have a large number of unsaturated sites (such as boundary sites, step sites, and defects) on the surface. Density functional theory (DFT) calculations showed that rough surfaces with unsaturated sites required lower activation energy to form important intermediates and showed better electrochemical activity for the CO_2RR.

Cu NWs also have excellent performance for the CO_2RR. 1D Cu NW catalysts can also be synthesized by the solvothermal method, and the morphology of ultrathin Cu NWs directly affects the selectivity for products in the CO_2RR. Ultrathin Cu NWs with a 20 nm diameter were prepared at high temperature for the CO_2RR [49], in which tris(trimethylsilyl)silane and oleylamine served as the reducing agent and solvent agent, respectively. The ultrathin Cu NWs showed high selectivity for CH_4, with an FE of

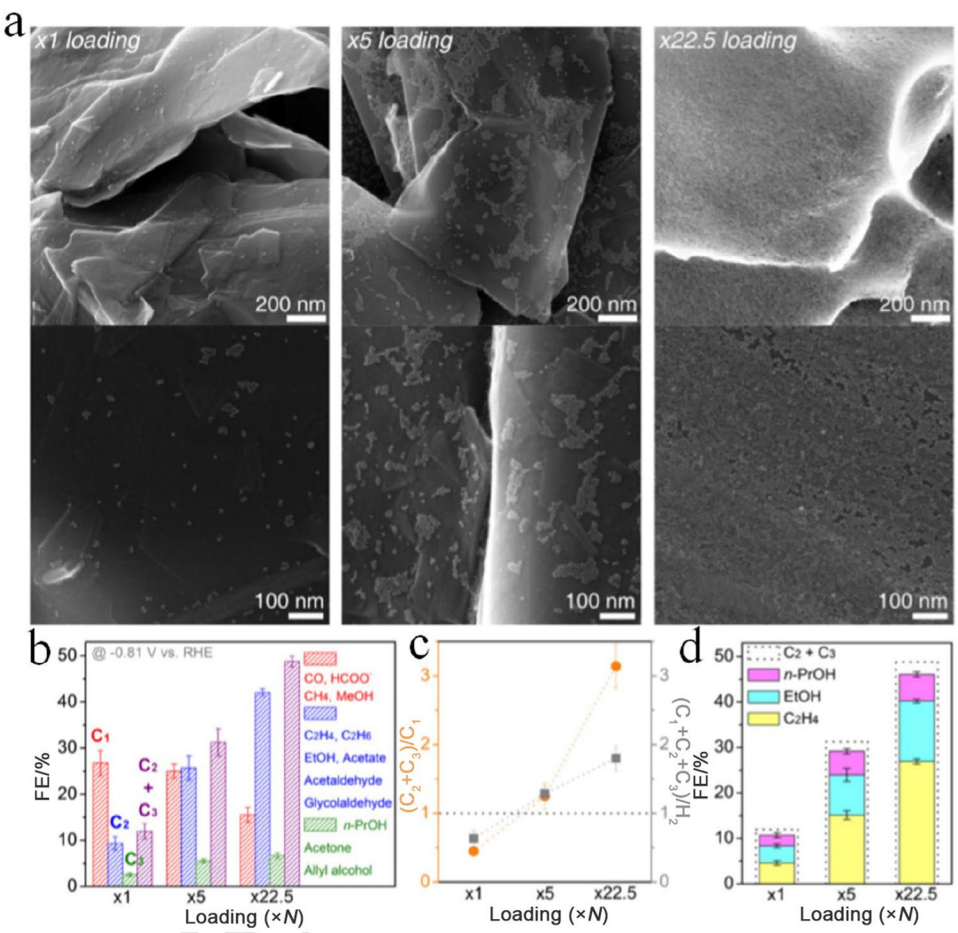

Fig. 2 Cu NP ensembles of various densities and their electrocatalytic activity. **a** SEM images of Cu NPs loaded on carbon paper supports at × 1 loading, × 5 loading, and × 22.5 loading. **b** FEs for C_1, C_2, and C_3 products. **c** Relative ratio of the FEs. **d** Ethylene, ethanol, and *n*-propanol FEs, with the dotted line showing the overall C_2–C_3 FE. Activity measured at −0.81 V versus RHE, using 0.1 M (1 M = 1 mol L^{-1}) $KHCO_3$ saturated under 101.325 kPa CO_2. The error bars shown in (**b**–**d**) are 1 SD from three independent measurements. Reproduced with permission from Ref. [54]. Copyright © 2017, National Academy of Sciences

55% for CH_4 at −1.25 V versus RHE, while the FE for other products was less than 5%. With increasing electrolysis time, ultrathin Cu NWs gradually became ultrafine Cu NPs. Meanwhile, the corresponding CO_2 electroreduction products also changed from CH_4 to C_2H_4 (other products such as CO and H_2 did not change with the variation in the morphology of Cu NWs). Annealing and electrochemical reduction were also employed to prepare Cu NWs. Highly dense Cu NWs as advanced electrocatalysts were prepared via a two-step synthetic strategy and greatly improved the CO_2 electroreduction efficiency [48]. CuO NWs prepared by oxidizing copper mesh in air were utilized as precursors for the synthesis of Cu NWs. By annealing them in the presence of hydrogen and applying a cathodic electrochemical potential method, CuO NWs were converted into Cu NWs with similar dimensions but distinct surface structures. The catalytic results showed that ethylene, ethane and ethanol could be detected at potentials more negative than −0.5 V versus RHE. The total FEs for C_2 products were approximately 25% between −0.7 and −0.9 V versus RHE, while methane or methanol was not observed at potentials lower than −1.0 V versus RHE [49]. A similar method was also used to prepare Cu NWs with a high grain boundary density [57]. First, $Cu(OH)_2$ NWs were grown by immersing copper foam in an aqueous solution of ammonium persulfate and sodium hydroxide at room temperature. Then, Cu_3N NWs were prepared by reducing $Cu(OH)_2$ NWs in a tube furnace, followed by an electrochemical reduction method in $KHCO_3$ solution saturated with CO_2 at −1.2 V versus RHE to yield Cu_3N-derived Cu NWs. Figure 3a shows the morphology of the Cu_3N-derived Cu NWs, which exhibited a rough surface as a result of electrochemical reduction. Meanwhile, abundant structural defects can be observed in Fig. 3b, and grain boundaries surrounded by (111), (200), and (220) atomic facets were obtained from aberration-corrected scanning transmission electron microscopy (STEM) images (Fig. 3c). Figure 3d shows that the current density of the Cu_3N-derived Cu NW catalyst was −50.6 mA cm^{-2} at −1.0 V versus RHE, which was significantly higher than that of Cu_3N NWs and Cu foam, indicating that the in situ reduced Cu NW catalyst had a higher CO_2 electrochemical reduction activity. Figure 3e reveals that three reduction products (C_1 and C_{2+} products from CO_2 reduction and H_2 from the HER) were obtained at −0.5 to −1.1 V versus RHE. The sum of the FEs for all hydrocarbon products increased from 63% to 90% with increasing potential. The maximum

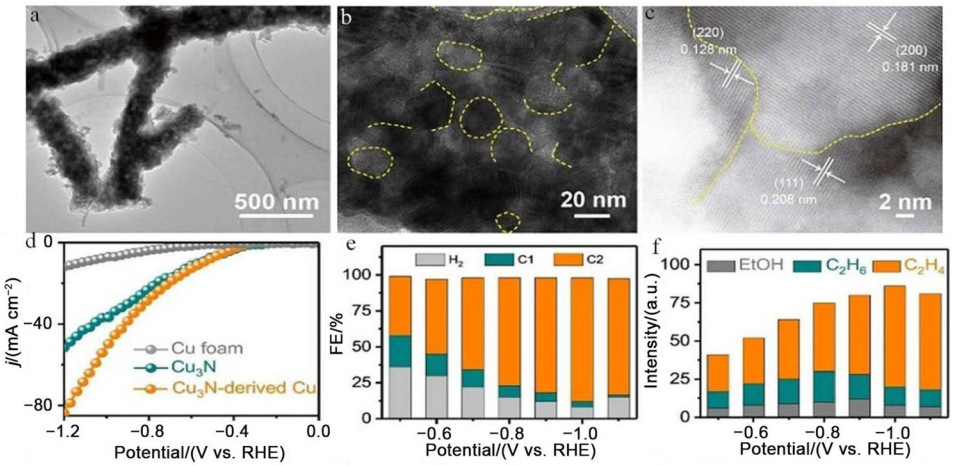

Fig. 3 Morphological characterization of Cu_3N-derived Cu NWs: **a** SEM image; **b** TEM image; **c** aberration-corrected STEM image. CO_2 electrochemical reduction characterization: **d** LSV curves measured in CO_2-saturated solutions at a scan rate of 10 mV s^{-1}; **e** FEs for H_2, C_1 and C_2 products at various applied potentials; **f** FEs for C_2H_5OH, C_2H_4 and C_2H_6 products at various potentials. Reproduced with permission from Ref. [57]. Copyright © 2019, John Wiley & Sons, Inc

FE for converting CO_2 to C_{2+} products with value-added, high-energy hydrocarbon was 86%, among which the FEs for ethanol, ethane and ethylene were 8%, 12% and 66%, respectively, as shown in Fig. 3f.

Compared with 1D and 2D Cu catalysts, 3D multilayer Cu catalysts have more active sites, which can increase the specific surface area of the catalyst and improve the mass transfer of the reaction. Therefore, such materials have great potential as a catalyst for CO_2 electroreduction. For example, a copper plate as a working electrode and a copper wire as a counter electrode were immersed in a solution containing copper sulfate and H_2SO_4. By using the electrodeposition method, a 3D porous Cu nanofoam catalyst was obtained [42]. Compared with the copper substrate, the FE for HCOOH increased from 3% to 29% with increasing thickness of the Cu nanofoam, and a trace amount of propylene products was detected. The improvement in the CO_2 electroreduction performance was attributed to the high surface roughness and multilayer pore structure of the Cu nanofoam catalyst. In the electrochemical deposition process, the morphology of Cu NWs was usually transformed into nanodendrites, which had a larger electrochemically active surface area (ECSA) and could produce a larger current density, thereby giving Cu nanodendritic structures excellent catalytic activity for the CO_2RR [58]. Novel Cu nanodendrites with a high ECSA were prepared by using a facile thermal-assisted method, in which the effects of the precursors, calcination temperature and time on the formation of the Cu nanodendrites were discussed. Compared with 1D Cu foam and Cu NPs, Cu nanodendrites showed a higher current density and a lower onset potential.

2.2 Bimetallic Cu-Based Catalysts

Although monometallic Cu catalysts have shown considerable catalytic performance toward the CO_2RR, the poor ability to adjust the adsorption energy of intermediate products on the single component results in limited activity and selectivity. Constructing bimetallic or multimetallic Cu-based catalysts is hailed as an effective approach to improve the electrochemical reduction of CO_2. The adsorption energy of intermediate products on the surface of the catalyst can be adjusted by changing the composition and proportion of metal elements. Compared with monometallic Cu catalysts, bimetallic Cu-based catalysts can change the atomic arrangement of the active centers involved in the reaction due to the interaction between the two different metals, thus altering the model through which the adsorbed species interacts with the surface. Studies have shown that Cu-based catalysts can regulate the electronic structure of the metal interface, which is an effective way to improve the electrochemical performance [59]. The reported bimetallic catalysts include Cu-Au, Cu-Zn, Cu-Ag, etc. [60–62]. Each metal catalyst displays distinct catalytic behaviors in the electrochemical carbon dioxide reduction process. The catalytic performance of the alloy can be adjusted by changing the composition of each metal in the alloy. Novel nanostructured Cu-Au alloys were prepared using template-assisted electrodeposition, where a nanoporous Cu film (NCF) served as the template. The results of linear sweep voltammetry (LSV) showed that the as-prepared Cu-Au alloy was active in catalyzing the CO_2RR [63]. The FE for methanol on $Cu_{63.9}Au_{36.1}$/NCF was 15.9%, which was approximately 19 times that on pure copper. The FE for ethanol was as high as 12%. Further analysis of the products showed that the FE for alcohols (methanol and ethanol) largely depended on the composition and nanostructure of the Cu-Au alloy. Pure Cu NPs of similar size were also tested for the CO_2RR, and the corresponding FEs for methanol (5.1%) and ethanol (4.6%) were higher than those on bulk Cu but still much lower than those on $Cu_{63.9}Au_{36.1}$/NCF. Similar pure Au NPs were not found to produce alcohols, suggesting that the Au component in the nanostructured Cu-Au alloy may greatly contribute to the enhanced conversion of CO_2 to alcohols. The performance of the catalyst varies with the composition and morphology of the catalyst, which is applicable not only to monometallic

catalysts but also to alloy catalysts. Generally, due to the inconsistency of crystallographic constants, lattice strain will be generated after introducing another metal into Cu-based catalysts to form alloys or bimetallic interfaces, which will further influence the geometric structure and electronic structure on the surface of the catalyst [64]. Physical mixing of Cu and Ag at the desired atomic ratios was used to prepare CuAg bimetallic electrodes under Ar in a vacuum arc furnace. The as-prepared CuAg bimetallic electrodes consisted of Cu and Ag crystallites. Compared with the Cu catalyst, the Cu-Ag alloy catalyst could convert CO_2 to C_2 products, and the selectivity of the alloy catalyst for C_{2+} products was significantly improved [65]. The incorporation of Ag into Cu could be proven to cause lattice strain in Cu, which would lead to a shift in the valence band structure and a decrease in the oxygen-philicity of Cu, thus changing the adsorption of intermediates, promoting mass transfer and improving the catalytic performance of the catalyst. However, Cu enrichment would occur on the surface of the Ag-rich bimetallic catalyst during the CO_2RR process due to the CO adsorbate-induced segregation of Cu initially dissolved in the Ag phase. The distribution of products on the stable CuAg bimetallic electrodes showed that CO was mainly generated on the Ag domain surface, while the reduction of CO occurred only on the Cu domain surface. Compared with pure copper, the production of H_2 on the Cu-Ag alloy catalyst was inhibited by approximately 75%. Although the inhibition of the HER could not suppress the ability of the Cu domain to generate products derived from CO, the distribution of the products was in favor of carbonyl products at the expense of hydrocarbons. Based on this strategy, Cu-Ag alloys were prepared by the electrodeposition method. The Cu-Ag alloys displayed much higher electrocatalytic performance than Cu metal. Cu-Ag NWs were formed by adding the additive 3,5-diamino-1,2,4-triazole (DAT) in the electrodeposition process [66] (Figs. 4a–4c). Compared with the Cu-Ag alloy synthesized without the additive DAT, the mixture of Cu and Ag atoms in the sample prepared in the presence of DAT was more uniform. The as-prepared Cu-Ag NWs showed higher activity and selectivity toward the reduction of CO_2 into C_{2+} products. Figure 4d shows that the alloys exhibited the best electrocatalytic performance for carbon dioxide when the Ag content was 6%, and the FEs for ethylene and ethanol reached 60% and 25%, respectively.

Combining Cu and other metals to form bimetallic catalysts is also an effective method to regulate the catalytic activity and selectivity for the CO_2RR. Three solid-solution types of CuPd were prepared with the same composition and different atomic arrangements of NPs (disordered, ordered and phase-separated arrangements) [29]. The preparation of disordered, ordered and phase-separated CuPd catalysts was as follows. Briefly, the disordered type of CuPd was synthesized by reducing a mixture of $Pd(HAc)_2$ and $Cu(HAc)_2$ (with a molar ratio of Cu(II):Pd(II) = 1:1) in a solution of 2-ethoxyethanol using $NaBH_4$ as the reducing agent. $Cu(HAc)_2$ was mixed

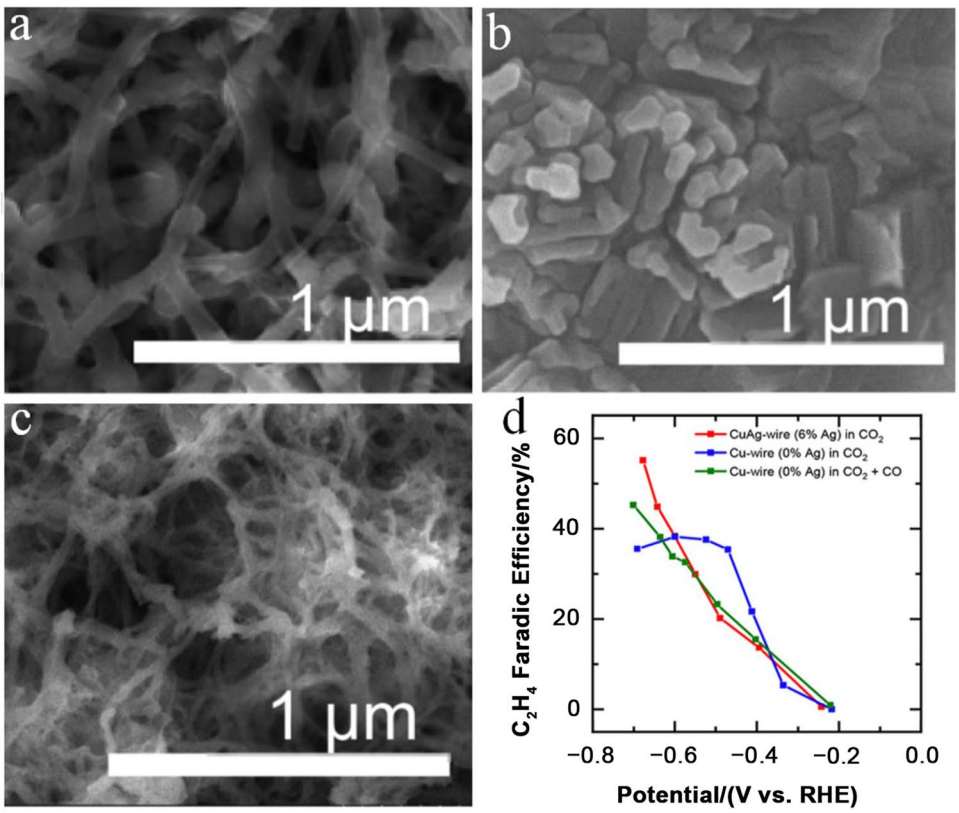

Fig. 4 SEM images of **a** Cu wires (0% Ag) electrodeposited with DAT, **b** CuAg poly (6% Ag) electrodeposited without DAT, and **c** CuAg wires (6% Ag) electrodeposited with DAT, and **d** FEs for C_2H_4 production from Cu wires and CuAg wires in CO_2 and CO_2 + CO. Errors are ca. ± 5%. Reproduced with permission from Ref. [66]. Copyright © 2018, American Chemical Society

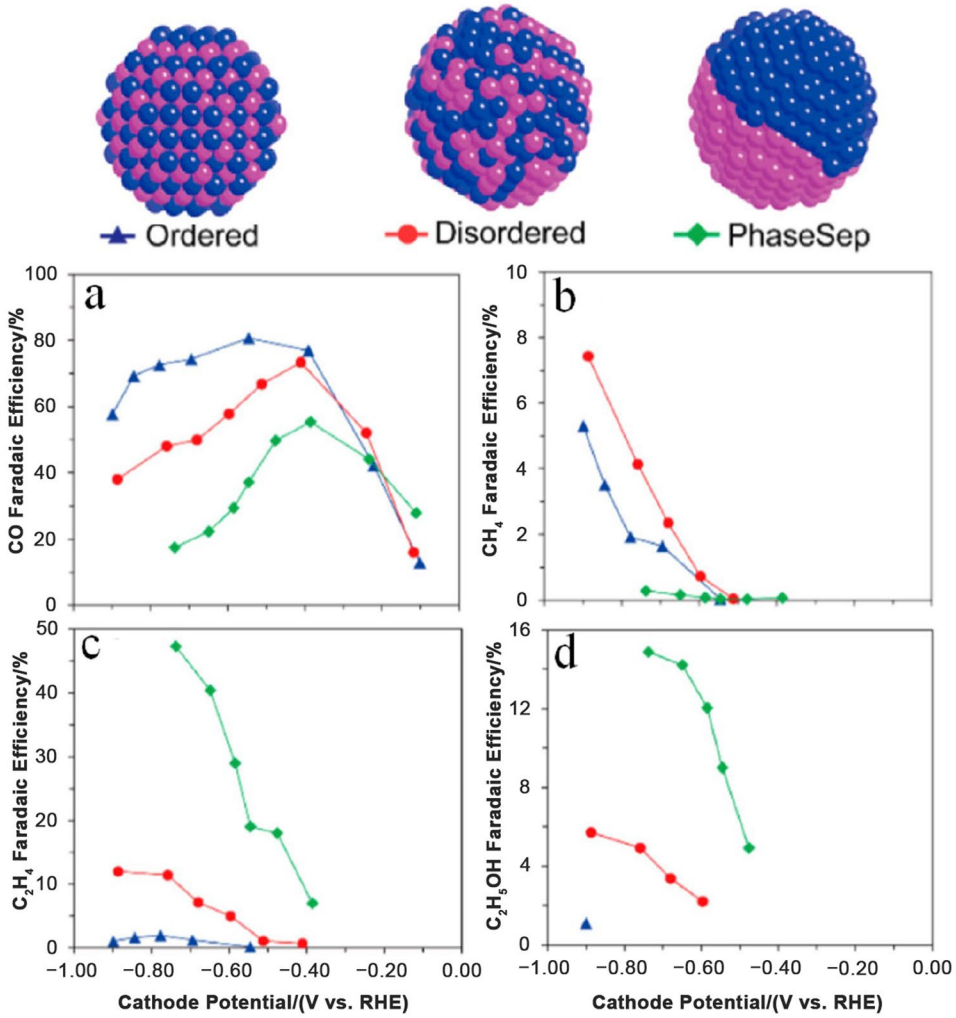

Fig. 5 FEs for **a** CO, **b** CH_4, **c** C_2H_4, and **d** C_2H_5OH of bimetallic Cu-Pd catalysts with different mixing patterns: ordered, disordered and phase-separated. Reproduced with permission from Ref. [29]. Copyright © 2017, American Chemical Society

with a solution containing $Pd(HAc)_2$ acetone solution and 2-ethoxyethanol, and then, $NaBH_4$ was added with stirring to obtain phase-separated CuPd. The phase-separated type of the CuPd nanoalloy was annealed to accelerate the atomic displacement to form the ordered type of CuPd. Figure 5 shows the three atomic arrangements of the ordered, disordered and phase-separated Cu-Pd nanocatalysts. The electrochemical results demonstrated that the FEs for ethylene and ethanol on the phase-separated CuPd NPs were much higher than those on the ordered and disordered CuPd NPs, while the FE for methane was much lower than that on the ordered and disordered CuPd NPs (Figs. 5a–5d). For phase-separated CuPd NPs, adjacent Cu atoms promoted CO dimerization, while for ordered and disordered CuPd NPs, CO that adsorbed on Cu atoms could combine with oxygen atoms that adsorbed on Pd atoms to form the CHO intermediate and further hydrogenate to generate methane. The selectivity for the CO_2RR was related to the composition of the bimetallic catalysts as well as the arrangement of the bimetal. Among the many Cu-based alloy catalysts, only copper palladium alloy could catalyze highly selective electroreduction of carbon dioxide to ethylene. Most of the Cu-based alloy catalysts always maintained the copper product selectivity. For example, a Cu-Au alloy catalyst converted carbon dioxide to carbon monoxide, and the FE for ethylene decreased with decreasing Cu composition of the catalyst.

In practical applications, designing catalytic materials by combining a variety of nonprecious metals in the form of alloy or polyphase Cu-based catalysts is a cost-effective approach. The introduction of a second metal not only regulates the selectivity of the reaction for C_1 and C_{2+} products but also adjusts the selectivity of the reaction for different C_{2+} products. Cu-Zn bimetallic catalysts with three compositions were prepared by introducing different contents of Zn [61] into Cu_2O, followed by an in situ electrochemical reduction process. Further characterization revealed that Cu and Zn did not form an alloy but existed in two phases. The electrochemical CO_2 reduction performance was measured, and the ratios of the FEs for ethanol to ethylene on the three Cu-Zn bimetallic catalysts were compared with those on pure

Cu and pure Zn. The results showed that pure Zn could not produce ethylene or ethanol, and the main product was CO. The ratio of ethanol to ethylene on the pure Cu electrode was 0.48. The ratio of ethanol to ethylene on the Cu-Zn bimetallic electrodes increased with increasing Zn content, reaching the maximum value on the Cu_2Zn bimetallic electrode (the ratio was 6). Then, the researchers studied the underlying mechanism and found that the FE for CO on the surface of pure Zn increased with increasing voltage, while on the Cu-Zn bimetallic electrodes, the FE for CO decreased when the voltage exceeded a certain value, which confirmed that Cu and Zn had a synergistic effect; in other words, CO generated on the surface of Zn NPs could migrate to the surface of Cu NPs and undergo dimerization to form C_2 products. However, the researchers did not explain why the introduction of Zn improved the selectivity for ethanol over ethylene but emphasized that similar results had been observed in previous Cu-Au bimetallic catalysts [19].

In addition to constructing metal alloy structures to realize an enhancement effect of Cu-based catalysts, alloy catalysts other than Cu-based catalysts can be fabricated that promote carbon-carbon coupling. For non-Cu metal, the binding energy can be adjusted to the appropriate range by forming alloys. Pd-Au, Ni-Ga and Ni-Al and other non-Cu-based bimetallic catalysts have shown the ability to catalyze electrocatalytic CO_2 reduction to C_2 and multicarbon products, but the corresponding FE is not high (< 5%) [67–70]. Electrode of Ni-Ga catalysts [69] with different proportions was prepared by the drop coating method, which could realize the products of CH_4, C_2H_4 and C_2H_6 at low overpotentials, but the selectivity for the products was poor. Although their selectivity was not high, they provided new insights for the design of non-copper-based electrocatalysts that could enable efficient electroreduction of CO_2 to C_2 products. In conclusion, by changing the composition and structure of the alloy catalyst and continuously optimizing its element distribution, the adsorption energy of the catalyst for intermediate products can be effectively adjusted, thus leading to the generation of target products.

2.3 MOFs and MOF-Derived Catalysts

MOFs are a kind of porous crystalline material composed of metal or metal clusters and organic ligands with functional groups (–COOH, –OH, $–NH_2$, –CN, etc.). The metal species and organic ligands are self-assembled by coordination bonds. In recent years, MOFs have attracted increasing attention in the field of heterogeneous catalysis due to their high specific surface area, postmodification and adjustable pore size and have been applied to the CO_2RR [71, 72]. Compared to inorganic microporous catalysts with high specific surface areas, the structure of MOFs is more flexible and can dynamically respond to temperature and pressure. The entire MOF is supported by coordination bonds and other weak interactions, such as hydrogen bonds, π–π stacking and van der Waals forces. Even under mild conditions, these MOFs can reversibly adjust their pore diameter according to external factors [73]. MOFs can be divided into two categories: (i) metal-organic polyhedra, in which transition metal ions are coordinated by electron-donor organic units of nitrogen or carboxylic acid, and (ii) zeolite imidazolate frameworks with the topological structure of zeolites. The method for the synthesis of the above-mentioned MOFs is simple, as most MOFs can be synthesized at low temperature with low cost and high yield, in which water (solvent) thermal conditions are the most common synthesis conditions. For the CO_2RR, MOF-related catalysts are mainly divided into two kinds: MOFs themselves as catalysts and MOF-derived materials that use an MOF as a precursor to prepare target catalysts, in which the metal centers are embedded in a carbon matrix in situ during high-temperature treatment of MOFs, such as metals, metal oxides and carbon materials loaded with metal NPs [74]. This structure provides excellent electron transfer performance between metal-metal oxides and carbon grids. Cu-MOF is a periodic network structure formed by Cu^{2+} and organic ligands [75]. Cu-MOF has the advantages of high porosity and large specific surface area and has been widely used for the CO_2RR [76]. The method for synthesizing Cu-MOF was reported to promote undercoordinated Cu sites with the aid of an MOF to optimize the CO_2RR activity of Cu clusters [77]. This performance tuning was achieved by contorting the symmetrical paddlewheel copper dimer of HKUST-1 into an asymmetric motif by heat treatment. Deformation of the copper dimer was achieved by separating benzene tricarboxylate and changing the calcination temperature. The formation of Cu clusters with low coordination number (CN) from distorted Cu dimers was observed by conducting electron paramagnetic resonance (EPR) and in situ X-ray absorption spectroscopy (XAS) experiments on HKUST-1 during CO_2 electroreduction, which exhibited a 45% FE for C_2H_4. $Cu_3(BTC)_2$ ($[Cu_3(\mu_6\text{-}C_9H_3O_6)_2]_n$) was synthesized through an electrochemical method and immobilized onto glassy carbon (GC) for the CO_2RR [78]. N,N-Dimethylformamide containing tetrabutylammonium tetrafluoroborate was used in a saturated CO_2 electrolyte to study CO_2 electrochemical reduction on the surface of a Cu-based organic framework membrane. CV studies indicated that the electrochemically generated Cu(I) material as a Lewis acid site was formed on the organic skeleton membrane of Cu-based MOFs and then adducted with CO_2 molecules to activate the reaction. The resulting CO_2^- intermediate could be coupled to oxalic acid through dimerization C–C bonding.

In recent years, direct carbonization of MOFs has been widely used to construct functionalized porous carbon and

metal-metal oxide composite materials. Cu-MOF-derived catalysts are widely used in the field of electrocatalysis. A study found that the metal coordination (Cu^{2+}) converted into CuO, Cu_2O and Cu_4O_3 during the electrolytic process. The in situ-derived Cu oxides could catalyze carbon dioxide reduction to formic acid and acetic acid with higher catalytic activity compared with single-component CuO, Cu_2O and Cu_4O_3, indicating the activity of the catalyst from the copper oxide and synergy between various components [79]. MOF-199 was modified with benzimidazole containing nitrogen and calcinated at different temperatures to obtain MOF-derived copper-nitrogen-doped carbon (Cu NPS-NC) catalysts [80]. The results showed that high contents of pyrrole N and Cu–N bonds were formed at a calcination temperature of 400 °C, which promoted the formation of ethylene and ethanol. At −1.01 V versus RHE, the FE for ethylene was 11.2%, that of ethanol was 18.4%, and the electrolysis could remain stable for more than 8 h. A copper oxide-derived carbon composite (OD-Cu/C) catalyst was synthesized via the carbonization of $Cu_3(BTC)_2$, converted CO_2 to alcohol with 45.2%–71.2% FE and exhibited high activity, high selectivity, and good stability for the CO_2RR [81]. From −0.1 to −0.7 V versus RHE, the total FE for ethanol and methanol, reached 71.2%, which was attributed to the synergistic effect of highly dispersed Cu metal centers and porous carbon supports. These results indicate that the catalytic activity and products of Cu-MOF-derived catalysts are greatly related to the calcination temperature, which may provide a new avenue for the design of MOF-derived catalysts.

Although the above materials have demonstrated good electrocatalytic activity, some disadvantages limit their application. For example, their surface area and adsorption ability are significantly reduced when exposed to moisture. In addition, most MOFs display poor electrical conductivity, and the narrow micropores of MOFs limit the rapid diffusion of gas in the pores [82, 83]. To solve these shortcomings, researchers proposed combining MOFs with various functional materials to form MOF-based composites. In MOF-based composites, the advantages of MOFs and various functional materials can be effectively combined, which can generate synergistic effects and compensate for the shortcomings of a single component. Therefore, MOF-based composites have great potential for electrochemical reduction of CO_2.

2.4 Other Catalysts

In recent years, single-atom catalysts (SACs) and nonmetallic catalysts (microorganisms, carbon nanomaterials and nonmetallic composites) have been gradually applied to the electrochemical reduction of CO_2 due to their abundant sources, low cost and environmental friendliness.

SACs The key of CO_2RR research is to design and develop efficient and inexpensive catalysts with high activity, high selectivity, high stability and significant inhibition of the HER. An SAC with a highly dispersed single-atom active center that could ensure high utilization of atoms is a new frontier in the field of catalysis [84, 85]. SACs refer to catalysts with excellent catalytic performance formed by uniformly dispersing low coordination active metals on a support, in which the metal achieves the maximum atomic utilization rate [86–88]. SACs have attracted much attention because of their unique electronic structure and geometric structure, showing excellent catalytic activity for many important chemical reactions (CO_2RR, CO oxidation reaction, hydrogenation reaction, OER, oxygen reduction reaction, HER, etc.). The geometric and electronic structures undergo distinct changes as the catalyst continues to shrink from the nanometer scale to the single-atom scale, becoming completely different from those of nanocatalysts. The concept of SAC was first proposed by Zhang and coworkers; in their study, Pt atoms were atomically dispersed on the surface of iron oxide nanocrystals without agglomeration [89]. SACs have obvious advantages over traditional catalysts and have attracted much attention in recent years for the CO_2RR due to their fully exposed active sites, high selectivity and maximum atomic utilization [90]. The preparation methods of SACs are usually pyrolysis and reduction. Theoretical calculations showed that SACs embedded in another metal nitride, carbide [91, 92] or nitrogen-doped carbon matrix [93, 94] could enable electroreduction of CO_2 into not only CO and formate but also multiple carbon products. A ferrous cluster supported on carbon doped with nitrogen could convert CO_2 to acetic acid, and the FE for acetic acid was 61% at −0.5 V versus Ag/AgCl, which showed that iron(II) in nitrogen coordination acted as a monatomic or polyatomic active site and could achieve C–C coupling synergistic with N to increase the catalytic activity of the CO_2RR. Single-atom Cu catalysts for the CO_2RR have also been reported. At present, most SACs mainly convert CO_2 to CO, and the design of SACs that can reduce CO_2 to hydrocarbons or alcohols still faces great challenges. The generation of C_2 and multicarbon products is closely related to the coverage of CO intermediates on the Cu catalyst surface, and catalysts with high selectivity toward CO_2 to CO conversion are already common [95–97]. Designing tandem catalysts to achieve $CO_2 \rightarrow CO \rightarrow C_2$ could be considered [98]. Single-atom Cu catalysts loaded [99] on mesoporous CeO_2 NWs could convert CO_2 into the deep reduction product CH_4 with an FE of 58%. The above products (CO, methanol and methane) are all C_1 products, while there have been few related systems that can synthesize C_2 and multicarbon products. The reason lies in the distance between the single-atom active centers, which makes effective promotion of the carbon-carbon coupling reaction difficult. If the surface density of Cu could be improved while maintaining the dispersion of the Cu active

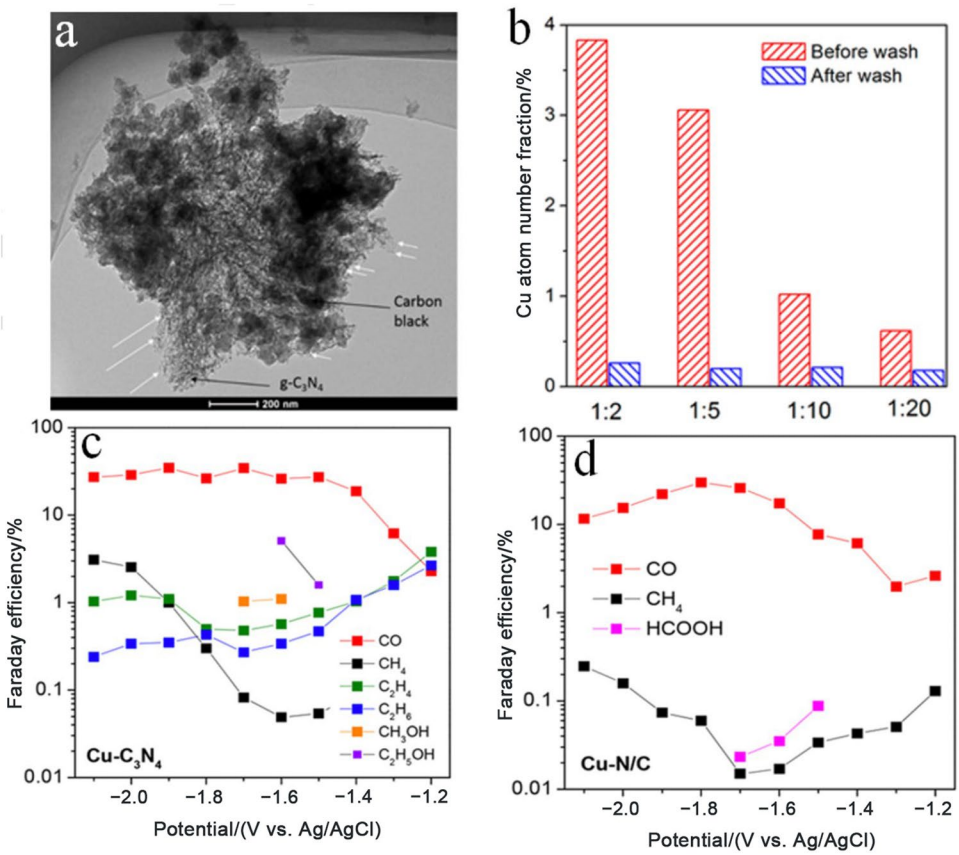

Fig. 6 **a** TEM image of a typical Cu-C_3N_4 electrocatalyst supported on carbon black; arrows indicate atomic Cu clusters. **b** Comparison of Cu concentrations in different Cu-C_3N_4 samples before and after an acid wash. **c** Measured FEs for various products on Cu-C_3N_4 and **d** Cu NC electrodes under different overpotentials. Reproduced with permission from Ref. [100]. Copyright © 2017, American Chemical Society

center at the atomic level, then C_2 and multicarbon products could be obtained. The method of preparing monatomic catalysts assisted by MOFs is very simple and efficient, and the as-prepared electrocatalysts showed higher activity and selectivity for the CO_2RR than most precious metal-based catalysts, with great potential for industrial application. Synthesis of Cu-C_3N_4 nanomaterials was accomplished by mixing different amounts of $CuCl_2$ aqueous solutions with dicyandiamide (DCDA) at room temperature [100]. The suspension was then mixed with carbon black pretreated with acid and annealed at 600 °C in N_2 to obtain Cu-C_3N_4 (Figs. 6a and 6b). Finally, the Cu-NC catalyst was prepared by annealing Cu-C_3N_4 powder at 900 °C in N_2, during which g-C_3N_4 decomposed and was converted into nitrogen-doped carbon coordinated with Cu. Cu single atoms were anchored on a C_3N_4 support for electrochemical reduction of CO_2 and showed excellent activity with a lower onset potential. Cu@C_3N_4 showed higher selectivity for C_2 products than Cu@N/C (Figs. 6c and 6d), which revealed that the molecular scaffold could serve as an additional active center for the CO_2RR and have a synergistic effect on the pathway that produces deeply reduced products. Although few SACs have been reported that could effectively improve the selectivity for C_2 products, these early explorations suggest that development of novel metal SACs and optimization of the interaction of metal atoms with the support and coordination elements may be an effective way to improve the product selectivity.

Microorganisms Microorganisms play an important role in biological electrochemical systems that efficiently treat organic wastewater and solid waste and solve environmental and energy problems. In addition, they can be used as catalysts for the catalytic electrochemical reduction of CO_2 to produce energy substances (methane and ethanol) and organic chemicals (formic acid, acetic acid, butyric acid, 2-carbonyl butyric acid, caproic acid and octanoic acid). The catalytic effect of microorganisms has been shown using methane bacteria, acetic acid bacteria, and methane bacteria particles [101]. Methanogens were first used as catalysts for the CO_2RR and to produce methane [101], which provided a new idea for the electrochemical reduction of CO_2.

Carbon nanomaterials Compared with metallic catalysts, carbon materials have attracted increasing attention for the CO_2RR because of their adjustable porous structure, high specific surface area, acid and alkali corrosion resistance and environmental friendliness. Carbon nanomaterials have the advantages of high conductivity, good stability and low price. Carbon-based materials are more tolerant to extreme conditions (such as strong acidic electrolytes) and exhibit higher stability than metal and metal oxide catalysts,

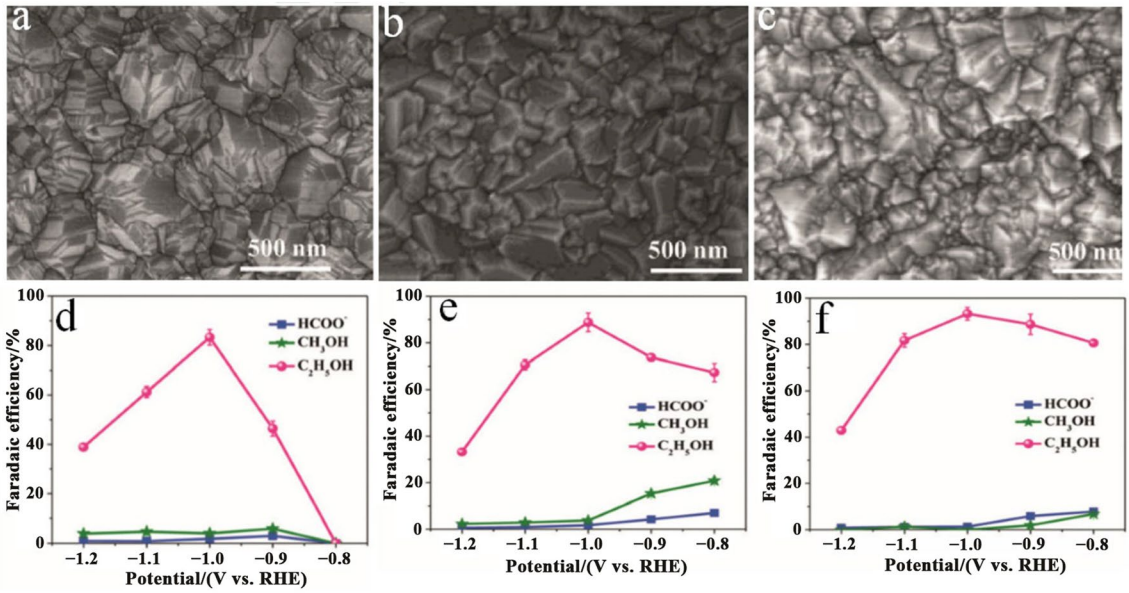

Fig. 7 SEM images of **a** BND1, **b** BND2, and **c** BND3, and FEs of **d** BND1, **e** BND2, and **f** BND3. Reproduced with permission from Ref. [104]. Copyright © 2017, John Wiley & Sons, Inc

which is one of the reasons why carbon-based materials have attracted much attention recently. They have the most potential to replace precious metals for electrochemical reduction. Based on these advantages, much research has reported the application of carbon materials in the electrocatalytic reduction of carbon dioxide. Hydrocarbons and their derivatives (alcohols, acids and aldehydes) are products of deep reduction of carbon dioxide, with high energy density and high added value, and are ideal products from electrocatalytic reduction of carbon dioxide. A nitrogen-doped nanodiamond/Si rod array (NDD/Si RA) film electrode was prepared by microwave plasma-enhanced chemical vapor deposition for the CO_2RR in $NaHCO_3$ aqueous solution and could quickly convert CO_2 to acetate with an onset potential of −0.36 V versus RHE, overcoming the limitation of low selectivity for the C_2 product [102]. The FE for CH_3COOH was as high as 91.8% between −0.8 and −1.0 V versus RHE. The electrochemical results and in situ infrared analysis showed that the main pathway for CO_2 reduction might follow the reaction path of $CO_2 \rightarrow CO_2^{\cdot-} \rightarrow (COO)_2^{\cdot} \rightarrow CH_3COO^-$. The excellent performance in carbon dioxide molecule conversion to acetic acid on the NDD/Si RA catalyst was attributed to the N-sp^3C species acting as the active sites and the high overpotential for hydrogen evolution. The N or N-C structure of metal-free carbon materials could promote the formation of C–C bonds. N-doped graphene quantum dots (NGQDs) with 0.7 and 1.8 nm thicknesses were synthesized through exfoliation and cutting of a graphene oxide (GO) precursor and in situ doping of N into a dimethylformamide (DMF) solvent at high temperature and pressure [103]. The NGQDs could catalyze the electrochemical reduction of carbon dioxide to C_{2+} hydrocarbons and oxygenates with low overpotentials, high FEs and high current densities. The sum of the FEs for the CO_2RR was up to 90%, and the selectivity for ethylene and ethanol was 45%, which was comparable to that of Cu-based NP electrocatalysts. B/N codoped diamond (BND) films were prepared on silicon wafer surfaces by the chemical vapor deposition method [104], with BND1, BND2 and BND3 obtained with the same B_2H_6 content but different N_2 levels. Figures 7a–7c show the surface morphology of the as-prepared BND electrodes, which reveals that the BND films were composed of pyramidal NPs covering the entire substrate. A polyhedral diamond crystal with clear edges and corners could be observed on BND1, as shown in Fig. 7a. The FE for C_2H_5OH was 93.2%, which was significantly enhanced relative to the values reported for other electrocatalysts. Figures 7b and 7c show that twin crystals appeared at the grain boundaries of BND2 and BND3 as the N content of BND increased. Figures 7d–7f show that the BNDs preferentially convert CO_2 to C_2H_5OH. Interestingly, the production rate of C_2H_5OH significantly increased as the potential negatively shifted from −0.8 to −1.1 V versus RHE (the maximum production rate was at −1.0 V vs. RHE), in which the measured production rate of C_2H_5OH was 9.3 times, 17.5 times and 51.0 times that of CH_3OH and 11.4 times, 16.1 times and 12.9 times that of $HCOO^-$ for BND1, BND2 and BND3, respectively. The production rate of C_2H_5OH on BND2 was higher than that on BND1 under each potential applied but lower than that on BND3 at −0.8 to −1.0 V versus RHE, which indicated that increasing the N content of BND to some extent could

facilitate C_2H_5OH production. BND2 had a slightly higher production rate of C_2H_5OH than BND3 at −1.1 to −1.2 V versus RHE. A contrast experiment showed that the main product on the nanodiamond electrode doped only with B was formaldehyde, which indicated that N doping played a key role in the generation of multicarbon products. The main product of the N-doped catalyst was acetic acid instead of ethanol, indicating that there was a synergistic effect between N and B. If the N-doped nanodiamond was replaced by an N-doped graphite carbon material, then the main products were CO and formic acid, which indicated that the diamond material itself also played a decisive role. Experimental analysis and DFT calculations showed that the high activity and selectivity of BND for C_2H_5OH mainly originated from the synergistic effect of B and N codoping and the good balance of N content and H_2 evolution potential.

3 Reaction Mechanism for the CO_2RR to C_{2+} Products

Compared with the process of generating C_1 products via the CO_2RR, the generation of C_2 and multicarbon products involves the C–C coupling reaction, which is more complex in dynamics and is not conducive due to the competition with the HER reaction, thus leading to lower FE. First, C–C coupling reactions usually have relatively high activation energy and compete with the process of forming C–H and C–O bonds. Second, the thermodynamic potentials for the formation of CO intermediates and the formation of C_2 and multicarbon products are quite different. Sixteen products of CO_2 electrocatalytic reduction were detected on the surface of Cu electrodes [105] in $KHCO_3$ aqueous solution. At present, the FE of the catalyst in the laboratory stage can reach over 95%, while the FE for the C_2 product is only approximately 60% [105], and the maximum FE for the C_3 product is 21% [106]. Considering the requirements of high FE and high current density, the most promising target products are carbon monoxide, formic acid and ethylene at present. In addition, as an important solvent, liquid fuel and raw material for the production of many chemical products, ethanol was also an expected C_2 product of electrocatalytic CO_2. The C–C coupling reaction requires optimal affinity between the catalyst and CO because there is a balance in the binding affinity. On the one hand, the surface of the catalyst needs to have a strong enough adsorption energy for CO to ensure that CO has a sufficiently high coverage on the surface and further coupling occurs. On the other hand, the activation energy barrier of the coupling reaction increases with increasing CO adsorption energy on the surface, which greatly limits the range of alternative catalysts. Among many metals, the Cu surface has a suitable affinity for CO, and Cu-based catalysts can catalyze CO coupling [107]. However, research on the reaction mechanism for the CO_2RR on Cu electrodes is still in the early stage, and the different reaction pathways proposed match different experimental results and produce different products. Due to the variety of carbon dioxide reduction products on copper catalysts, improving the selectivity and FE of copper catalysts and realizing highly selective reduction of carbon dioxide to C_2 products have become the focus of many studies. The multielectron transfer reaction and the complexity of the reduction products limit further research on the electrocatalytic reduction mechanism of CO_2. In situ characterization and quantification of adsorption intermediates is a bottleneck to understanding elementary reactions. Therefore, the application of in situ electrochemical spectroscopy to characterize the adsorption intermediates of CO_2 electrocatalytic reduction and the construction of models of CO_2 electrocatalytic reduction based on possible adsorption products will become the key to deeply understanding the CO_2 conversion process to hydrocarbons. Understanding the formation mechanism of C_2 is very important for conducting research on electrocatalytic materials and electrolyte materials for specific target products. Therefore, the following focuses on the mechanism for the electrocatalytic reduction of CO_2 to C_2 products.

CO_2 is reduced by electrocatalysis to produce different products, which involves the transfer of multiple electrons. Table 1 lists some common reduction products and the corresponding standard reduction potential. Among the various products, CO and formic acid (or the formic acid ion) are the most common because their production only involves two electron transfers, while the others are deep reduction products. Deep reduction products can be obtained with CO gas as a raw material, but not with other small carbon molecules [108]. Therefore, CO is generally believed to be the most critical intermediate in the process of CO_2 reduction to C_2 and multicarbon products. There have been many reports on electrocatalytic CO_2 reduction to obtain C_1 products, and the relevant mechanistic studies are relatively clear [109]. CO is an important intermediate for the formation of C_2 and multicarbon products. To form C–C bonds, two CO molecules should be sufficiently close to the surface of the catalyst for further C–C coupling reactions. Thus, the formation of C_2 and multicarbon products is more challenging than that of C_1 products. The complexity of the mechanism for the CO_2RR brings great difficulties to the development of efficient catalytic materials. To understand the reduction pathways of CO_2 on the surfaces of different catalysts and then provide new insights for the development of catalysts, researchers have carried out many experiments and theoretical calculations and have achieved some progress.

3.1 Mechanism of CH_2 Carbine Dimerization

Figure 8 shows that when CO adsorbs on the surface of the Cu catalyst, subsequent hydrogenation could occur either on

the C atom to generate *CHO intermediates or on the O atom to generate *COH intermediates. Then, further hydrogenation dehydrates these intermediates to form *C intermediates, followed by the formation of $*CH_2$ carbine intermediates, which are coupled to form ethylene. The *C intermediate involved in this mechanism can be exactly explained by the experimental results [108], in which the graphite carbon signal was detected on the surface of the Cu catalyst by X-ray photoelectron spectroscopy and Auger electron spectroscopy in a CO_2 reduction experiment. The adsorbed state CH_{2ads} was confirmed to form by the hydrogenation of CO_{ads} and regarded as the common intermediate to form CH_4 and C_2H_4, where CH_4 was formed by the double proton-electron transfer reaction, and C_2H_4 was formed by dimerization and CO embedding. Through DFT calculations, the conclusion was obtained [110] that the generation of ethylene at a more negative potential (−1.15 V vs. RHE) could undergo the reaction path of "CH_2 carbine dimerization".

3.2 Mechanism of CO Dimerization

For the C–C coupling mechanism of CO_2 electroreduction to C_2H_4, the current general understanding is that CO_2 is first reduced to *CO, and then, two *CO intermediates are directly C–C coupled to form a *OCCO intermediate, which can be further hydrogenated and deoxygenated to form C_2H_4. Recent studies showed that CO_{ads} was the key intermediate of CO_2 electrocatalytic reduction, and the stability in the reduction process was related to the conversion activity of the CO_2RR. For the first time, the influence of pH on the mechanism was taken into consideration. The formation of CHO_{ads} was found to depend on pH, while the formation of the CO_{ads}-CO_{ads} dimer was independent of pH. CO_{ads}-CO_{ads} and CHO_{ads} intermediates would be further reduced to form C_2H_4 in the reaction process. The adsorption structure of the CO dimer on the Cu(100) facet and the subsequent reduction to ethylene or ethanol were deduced through theoretical calculations [32]. The characteristic of this mechanism was that the reaction pathway could occur at a relatively low potential (−0.4 V vs. RHE). Two CO molecules that adsorbed on the Cu(100) facet were coupled via an electron transfer process to form a $*C_2O_2^-$ dimer. The adsorption structure of the dimer on the Cu(100) facet was proposed as one C atom and one O atom separately bound to two Cu atoms, and the negative charge was mainly distributed on the CO groups that were not bonded to the surface. Along the pathways from CO dimerization to C_2 products, O atoms with more negative charges were first hydrogenated to form a *HOCCO intermediate, in which the C–C bond length was 146 pm, close to the value of a single C–C bond. The intermediate was further hydrogenated and dehydrated to form *CCO, and the C–C bond length was 133 pm, indicating that the C=C bond was formed. The next three hydrogenation steps occurred successively to form the important intermediate $*CH_2CHO$. There were two possible pathways for subsequent hydrogenation reactions: (i) if the C=C bond was retained, then hydrogenation occurred on the C atom adjacent to the O atom, resulting in ethylene desorption; (ii) if the C=C bond was broken, then the $*CH_3CHO$ intermediate was generated and then went through two steps of hydrogenation to produce ethanol, in which the $*CH_3CHO$ intermediate was also detected through in situ infrared spectroscopy [111]. By comparing the in situ infrared absorption spectra on the Cu(100) and (111) facets under an Ar atmosphere and a CO atmosphere, the characteristic absorption band of the *HOCCO intermediate could be observed on the Cu(100) facet under the CO atmosphere, whereas this band was absent on the Cu(111) facet. DFT was used to simulate the dimerization of CO on Cu(100) and (111) facets [112],

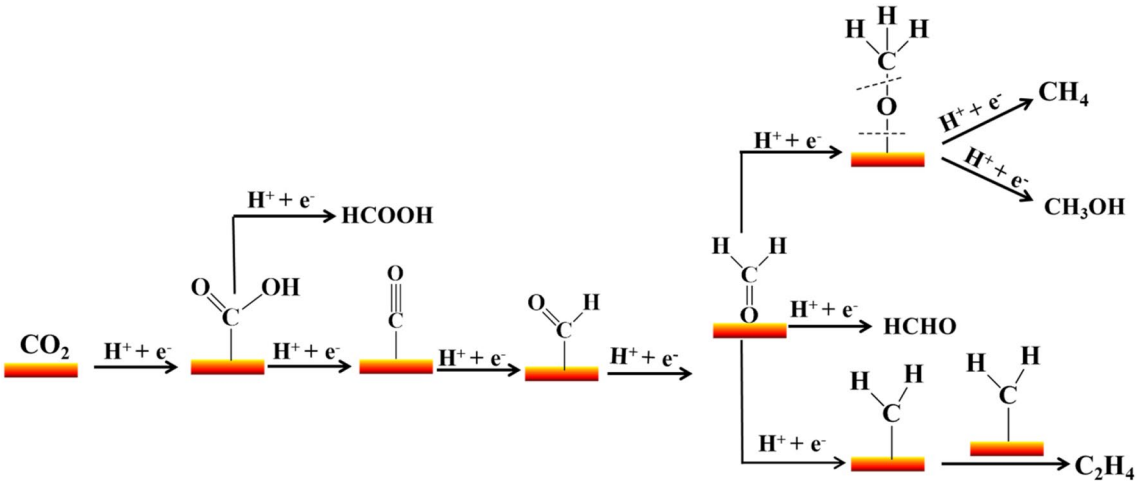

Fig. 8 Catalytic mechanism of ethylene formation via carbine dimerization from CO. Reproduced with permission from Ref. [108]. Copyright © 2013, John Wiley & Sons, Inc

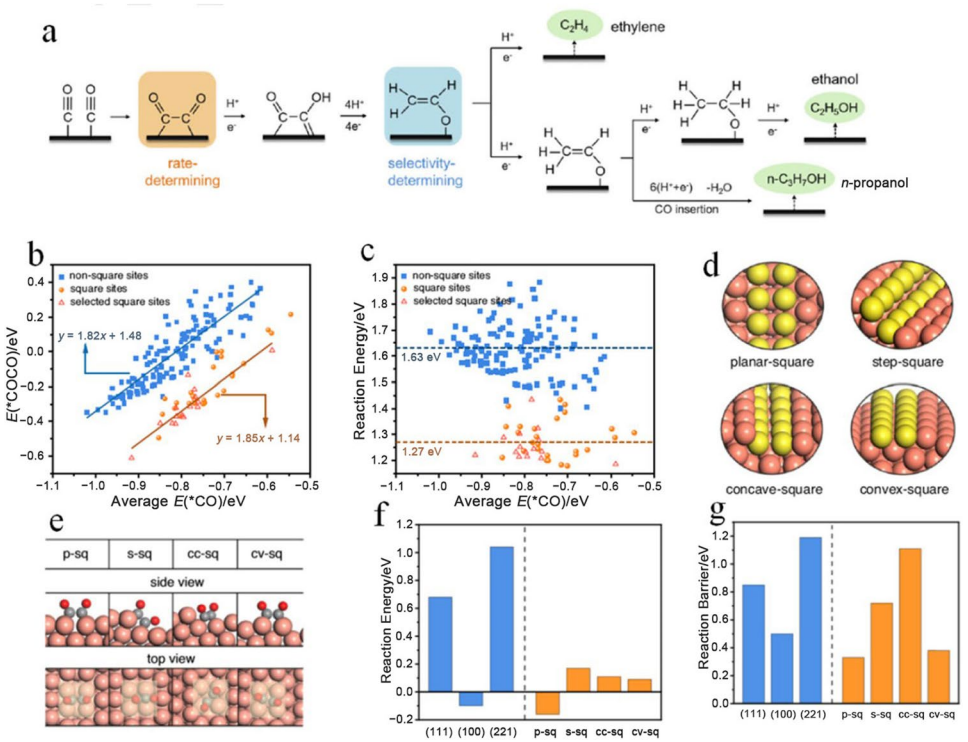

Fig. 9 **a** Reaction pathway for C_{2+} products in the CO_2RR. **b** Adsorption energy of *COCO as a function of the average adsorption energy of two adsorbed *CO. **c** Reaction energy (2*CO → *COCO) as a function of the average E(*CO) on these sites. **d** DFT periodic slab models of four square-like sites. **e** *OCCO configurations at these four sites (solvent molecules have been removed to show the adsorbate configurations). **f** Reaction energies and **g** barriers (2*CO → *COCO) on different DFT slab models under an appropriate electrochemical interface. Color code: brown—Cu; yellow—Cu at square-like sites; gray—C; red—O. Reproduced with permission from Ref. [116]. Copyright © 2021, Springer Nature

with the solvation effect of water molecules in the electrolyte taken into consideration. The simulation results showed that the energy barrier of CO dimerization was 0.68 eV on the Cu(111) facet and decreased to 0.33 eV on the Cu(100) facet, both of which were significantly lower than the simulated results under vacuum conditions [113], indicating that the solvation effect could significantly reduce the energy barrier of the dimerization reaction. In addition, the energy barrier on the Cu(100) facet was 0.3–0.4 eV lower than that on the Cu(111) facet, which was in line with the difference of at least 5 orders of magnitude in TOF. Thermodynamically, CO dimerization was exothermic on the Cu(100) facet and endothermic on the Cu(111) facet. For the next hydrogenation process, the energy barrier on the Cu(100) facet was also 0.4 eV lower than that on the Cu(111) facet, confirming that the CO dimerization reaction was highly sensitive to the surface structure of the catalyst, and the Cu(100) facet was more favorable in terms of both thermodynamics and kinetics. The presence of adsorbed CO_{ads} on the Cu surface was [114] observed by in situ infrared spectroscopy, and a further study confirmed that CO was one of the intermediate products in the reduction of hydrocarbon products. [115]. Realistic OD-Cu surface models were reported through simulation of the oxide-derived process by molecular dynamic simulations with a neural network (NN) potential [116]. Three square-like sites for C–C coupling were identified through the analysis of over 150 surface sites by high-throughput tests based on NN potentials and DFT calculations, in which Σ3 grain boundaries, such as planar-square (p-sq) sites and convex-square (cv-sq) sites, made the major contribution to the formation of ethylene. The step-square (s-sq) position is favorable for the formation of alcohol, which is due to the geometrical effect on the interaction between the stable acetaldehyde intermediate and the unstable Cu–O. Figure 9a shows the pathways for C_2 products. Solid-state experiments showed that the electroreduction of CO_2 to multicarbon products was independent of the standard hydrogen electrode (SHE), and the C–C coupling step without proton transfer was the rate-determining step (RDS), which meant that the C–C coupling rate determined the overall activity toward CO_2–C_{2+} product conversion on the OD-Cu catalyst. Both the vibration spectrum and kinetic model showed that *CO was the main intermediate on the Cu surface under reduction conditions. Then, 155 surface sites were randomly selected on the OD-Cu surface model to explore this dimerization process. The square orientation showed a significantly stronger *COCO binding energy. An additional 15 square sites were then selected from the OD-Cu surface to verify this trend. Figure 9c illustrates two different scaling relationships between the adsorption energies of the two binding states of *CO and *COCO intermediates at the nonsquare site and square site, where the energy on the square site was 1.27 eV, 0.36 eV lower than that on the nonsquare site. Therefore, the square site was more active for C–C conjugation. To accurately explore C–C coupling, plate models were introduced for precise DFT calculations, as shown in Fig. 9d. These models had similar chemical properties to the selected positions in the MD model. Calculations showed that the endothermic properties of the CO dimerization reactions

on these square structures were lower than those on the (111) and (221) facets under appropriate electrochemical interface conditions (Figs. 9e and 9f). The p-sq reaction energy was the lowest at −0.16 eV. In addition, the reaction barriers of C–C coupling at the p-sq, s-sq and cv-sq positions were 0.33 eV, 0.72 eV and 0.39 eV, respectively, which were much lower than the values of 0.85 eV and 1.19 eV on the (111) and (221) facets (Fig. 9g). Based on the above analysis, three active sites (p-sq, s-sq and cv-sq) on OD-Cu were found to be favorable for the production of C_{2+} products.

3.3 Mechanism of CHO + CO Coupling

DFT studies showed that the reaction energy of *CO directly coupled to *OCCO was very high (~ 1.9 eV). However, the hydrogenation of *CO to *CHO required a relatively low reaction energy (0.79 eV), and further C–C coupling by *CHO intermediates was also thermodynamically favorable. CHO_{ads} was formed through C–O bond fracture and subsequent hydrogenation [117], which was the main intermediate for CH_4 formation, as evidenced by online mass spectrometry analysis and the mechanism model. The formation of C_2 may be accompanied by the formation of CO bond dimers, and enediol was formed by further polymerization on the electrode surface, which was beneficial to the formation of C_2H_4. The mechanism of CO_2 electrocatalytic reduction on a Cu single-crystal surface was studied through DFT [108, 118], which further confirmed that CHO_{ads} was the main adsorption intermediate for CO_{ads} conversion to CH_4 and C_2H_4. The reaction path was calculated at a more negative potential (−1 V vs. RHE), and different mechanisms were found for the C–C coupling process under these conditions [119]. CO adsorbed on the surface of Cu(100) and then underwent hydrogenation and reduction to form a *CHO intermediate, followed by reaction with CO to form *COCHO, and thus, a carbon–carbon bond was formed. Subsequent hydrogenation could occur on β-C atoms with ethylene, followed by multiple steps. Hydrogenation could also occur on the α-C atom to produce glycolaldehyde, which could be further reduced to ethanol. The activation energy barrier for the previous process was slightly lower, which explained why the selectivity and FE for ethylene were usually several times higher than those for ethanol in experiments [40]. This mechanism could also explain the formation of other C_2 products, such as acetaldehyde, ethylene glycol, glycolaldehyde, glyoxal and acetic acid. Combined with DFT calculations, a new C–C coupling mechanism was proposed, and the promotion mechanism of F on the Cu surface was clarified [120]. On the F-Cu catalyst, CO_2 generated C_{2+} products through a novel "hydrogen-assisted carbon-carbon coupling" mechanism. The fluorine modification not only facilitated activation of H_2O to generate active hydrogen species (*H) but also promoted adsorption and hydrogenation of CO to produce *CHO intermediates, which could then be easily coupled and reduced to produce C_{2+} products on the copper surface. Figure 10a shows that fluorine modification further reduced the reaction energy of *CO hydrogenation to *CHO (0.48 eV). In addition, other possible coupling modes, such as CO → COH → HOCCOH (Fig. 10b) and CO + CHO → OCCHO (Fig. 10c), were compared, and CO → CHO → OCHCHO was found to be the most favorable reaction path. The presence of *CO and *CHO intermediates in the reaction process was further confirmed by in situ infrared spectroscopy to certify the hydrogen-assisted carbon-carbon coupling reaction mechanism. This broke the traditional understanding of the formation of C_{2+} products by *CO dimerization and illustrated the obvious advantages of C–C coupling by *CHO from theoretical calculations and in situ spectroscopy. This study not only provided a new strategy for the design of high-efficiency CO_2 electrocatalytic reduction catalysts but also opened up an avenue to regulate the selectivity for C_{2+} products through the discovery of the new mechanism of "hydrogen-assisted carbon-carbon coupling".

4 Strategies to Improve Catalysts

In the CO_2 electrocatalytic reduction process, controlling the adsorption energy of the key CO intermediate product on the surface of catalysts through the design of catalysts is an important approach to realize selective reduction of CO_2 to C_{2+} products. In recent years, many studies have made important progress in the aspects of surface facets, interface engineering, strong metal-support interactions and surface modification.

4.1 Surface Facets

The exposed crystal facet of Cu-based catalysts has a great influence on product selectivity because nanocrystalline catalysts with different crystal facets have different geometrical and electronic structures and thus exhibit different catalytic behaviors. The surface of Cu NPs is a combination of low index and low coordination site surfaces, corners, edges and defects. Cu nanocatalysts with different morphologies can expose different crystal facets, which affect the reactivity of the catalyst for the CO_2RR. High-index facets are often associated with high-density step atoms, kinks and side sites with low CNs, which make them highly active reaction sites that can easily break chemical bonds [121]. The facet of metal nanocatalysts affects the periodic structure of the atomic arrangement, the metal bond energy, and the adsorption and binding energies of various intermediates in the electrocatalytic reduction of CO_2, which will inevitably have an important impact on the catalytic performance for the electroreduction of CO_2. Many studies have shown that ethylene is more likely to form on the Cu(100) facet and that

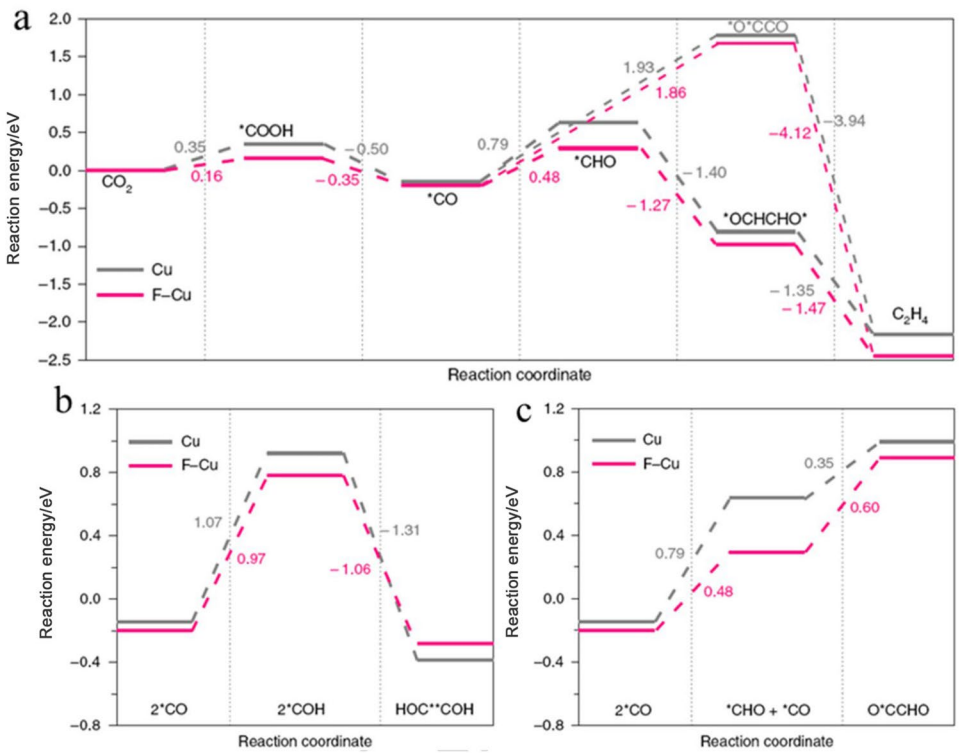

Fig. 10 **a** Reaction energy diagram for the CO_2RR to C_2H_4 on Cu(111) and F-Cu(111) facets, either via a direct *CO dimerization pathway or *CO hydrogenation to *CHO followed by a dimerization pathway; **b** reaction energy diagram for *CO hydrogenation to *COH and subsequent dimerization to HOC**COH on Cu(111) and F-Cu(111) facets; **c** reaction energy diagram for *CO hydrogenation to *CHO and subsequent coupling with another *CO to O*CCHO on Cu(111) and F-Cu(111) facets. Reproduced with permission from Ref. [120]. Copyright © 2020, Springer Nature

methane is more likely to form on the Cu(111) facet based on the surface of a single-crystal Cu catalyst [122, 123]. The Hori group [122] systematically investigated single-crystal Cu with high-index facets, i.e., Cu-[n(100)×(111)], Cu-[n(100)×(110)], Cu-[n(111)×(100)], Cu-[n(111)×(111)] and Cu-[n(110)×(100)], in 0.1 mol L^{-1} $KHCO_3$ solution and found that ethylene was the main product on the surface of the Cu electrode based on the (100) terrace facet and that ethylene production could be further facilitated by the introduction of (111) or (110) steps on the (100) facet. The ethylene to methane FE ratio was approximately 10 based on the (711) facet, while it was only 0.2 based on the (111) facet. Through electrochemical scanning tunneling microscopy (EC-STM) and differential electrochemical mass spectrometry (DEMS), the properties of monocrystalline Cu with the (100) facet were compared with those of the Cu(100) facet reconstructed by polycrystalline Cu. The results showed that no ethanol was detected on either of the catalysts with the Cu(100) facet and the Cu(100) facet reconstructed by polycrystalline Cu [124]. However, the Cu(100) facet reconstructed by polycrystalline Cu was reconstructed into a (511) high-index facet after 20 redox cycles in 0.1 mol L^{-1} KOH solution, which showed the ability to electrochemically convert CO_2 to ethanol with a 31% FE, while no methane or ethylene formation was observed. These studies strongly confirmed that the introduction of (111) or (110) steps on the Cu(100) facet to form a high-index facet was conducive to promoting the C–C coupling reaction. The adsorption energies of important intermediates on the face-centered cubic (fcc)-Cu(111), (100) and (211) facets were compared for the CO_2RR based on DFT calculations, and the catalytic performance was further validated [125]. The binding energies of all intermediates except O on the various facets followed the sequence: the Cu(211) facet > the Cu(100) facet > the Cu(111) facet. Based on the binding energy relationship, the authors further calculated the catalytic activity of CO_2 electroreduction to CH_4 on these facets. Interestingly, the Cu(211) facet had the highest catalytic activity, while the Cu(111) facet showed the lowest catalytic activity for producing CH_4. The Cu(111) and (100) facets for the CO_2RR were also compared, and the two different reaction mechanisms of hydrocarbon formation by CO_2 reduction were confirmed [123]. In the first reaction pathway, the same intermediate was found in the formation of CH_4 between the Cu(111) and (100) facets, which preferentially occurred on the (111) facet or step facet of the Cu nanocatalyst. In the second pathway, CO_2 was selectively reduced to C_2H_4 by forming a CO monomer adsorbed on the Cu(100) facet. Cu catalysts with the Cu(100) facet could promote the C–C coupling reaction, so the design of Cu(100) facet catalysts has attracted intensive attention [126]. The surface of polycrystalline Cu NPs was smooth and showed similar activity and selectivity to Cu(100) facet NCs after three redox cycles in $KHCO_3$ and KCl solution [127]. Researchers have speculated that the initial polycrystalline Cu NPs underwent the process of Cu → CuCl → Cu_2O → Cu because they found that the polycrystalline Cu NPs still had no obvious morphological characteristics after redox cycling

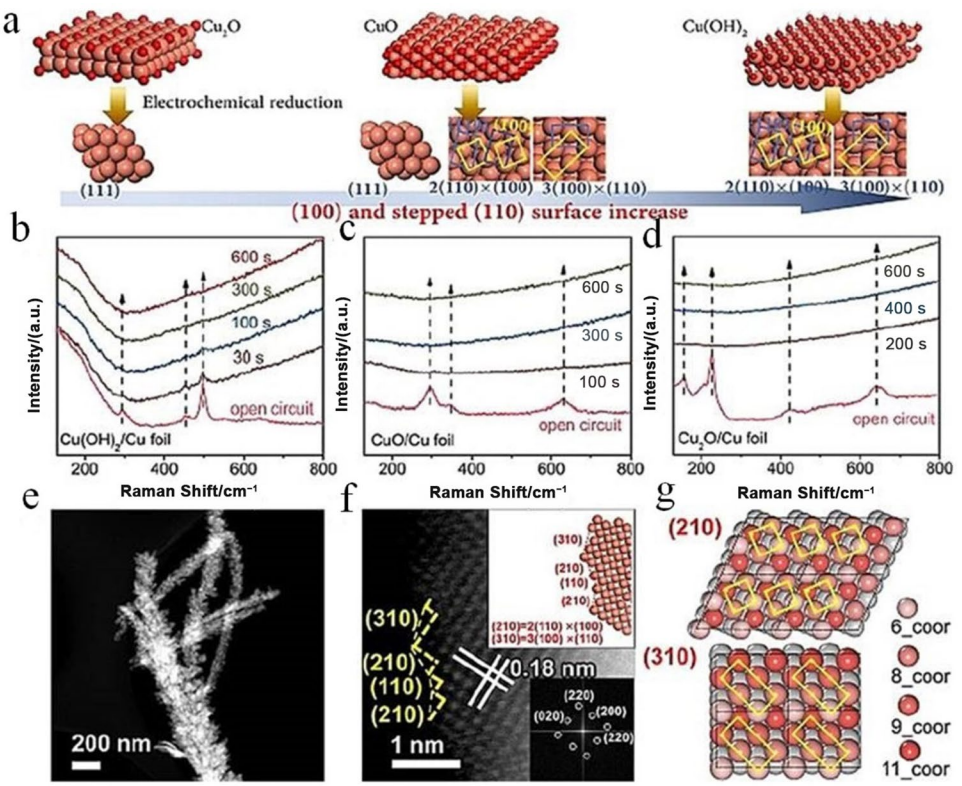

Fig. 11 Structure characterization of catalysts. **a** Illustration of the preparation of $Cu(OH)_2$-D/Cu foil, CuO-D/Cu foil, and Cu_2O-D/Cu foil; in situ Raman spectra of **b** $Cu(OH)_2$/Cu foil, **c** CuO/Cu foil, and **d** Cu_2O/Cu foil in CO_2-saturated 0.1 mol L^{-1} $KHCO_3$ at −0.5 V versus RHE; **e** and **f** aberration-corrected high-angle annular dark-field (HAADF)-TEM images of $Cu(OH)_2$-D, and **g** models showing CNs of (310) and (210) facets; the yellow square marked area is the square Cu(100). Reproduced with permission from Ref. [128]. Copyright © 2021, John Wiley & Sons, Inc

treatment in $KHCO_3$ solution without KCl. They compared the performance of Cu NCs and polycrystalline Cu NPs for the CO_2RR and found that the onset potential of Cu NCs to produce ethylene was −0.6 V versus RHE, whereas that of polycrystalline Cu NPs was −0.75 V versus RHE. More interestingly, the product of methane was not observed on the Cu NC catalyst, while its yield was nearly two times that of ethylene on polycrystalline Cu NPs. Cu catalysts with different facets were studied based on the wave potential, and the selectivity for products was examined by using in situ online electrochemical mass spectrometry (OLEMS) technology. The obtained results confirmed that Cu NCs significantly improved the selectivity for C_2H_4 in the CO_2RR compared with Cu NPs with polycrystalline structures. Although copper could effectively electrocatalyze the reduction from CO_2 to C_{2+} products (C_2H_4, C_2H_5OH and *n*-propanol), the correlation between the activity and the active site was still unclear, which hindered further improvement in the catalytic performance. A Cu catalyst with abundant stepped Cu(110) sites and highly active Cu(100) sites was reported to efficiently catalyze the CO_2RR to C_{2+} products. Figure 11a illustrates that the catalysts of $Cu(OH)_2$/Cu foil, CuO/Cu foil and Cu_2O/Cu foil were placed in a CO_2-saturated 0.1 M $KHCO_3$ aqueous solution and reduced under a bias potential of −0.5 V versus RHE for ~ 800 s to prepare $Cu(OH)_2$-D/Cu foil, CuO-D/Cu foil, and Cu_2O-D/Cu foil [128]. In situ Raman spectroscopy was employed to investigate the reduction process (Figs. 11b–11d). Interestingly, the $Cu(OH)_2$-D/Cu foil exhibited a rougher structure due to the more substantial lattice change during the reduction of $Cu(OH)_2$ to metallic Cu, as shown in Figs. 11e and 11f. The Cu(100) facet dominant in Cu(310) and Cu(210) sites also inherited the nature of the stepped Cu(110) with low coordination (Fig. 11g). The electrochemical results for the CO_2RR confirmed that the stepped Cu(110) and Cu(100) sites in $Cu(OH)_2$-D/Cu foils were crucial for the selectivity/activity enhancement of C_{2+} products by comparing the properties of different copper hydroxide/oxide-derived copper materials, which showed that the Cu(110) facet promoted CO adsorption and that the Cu(100) facet promoted C–C coupling to C_{2+} products, as demonstrated by DFT calculations, in situ Raman spectroscopy and in situ attenuated total reflectance-surface enhanced infrared absorption spectroscopy (ATR-SEIRAS). The FE for C_2H_4 was 58%, and the total FE for hydrocarbons and alcohols was 87% in the flow cell.

The formation of abundant grain boundaries on the surface of copper-based catalysts is also beneficial to increasing the selectivity for C_{2+} in the CO_2RR. Nanocatalysts are mainly composed of grains and grain boundaries, which have important effects on the properties of nanomaterials. In nanopolycrystalline materials, the orientation of grains is different, and there is an interface between grains, which is called the grain boundary. Grain boundaries connect grains with different arrangement directions, and the arrangement of atoms transitions from one direction to another. Therefore, the arrangement

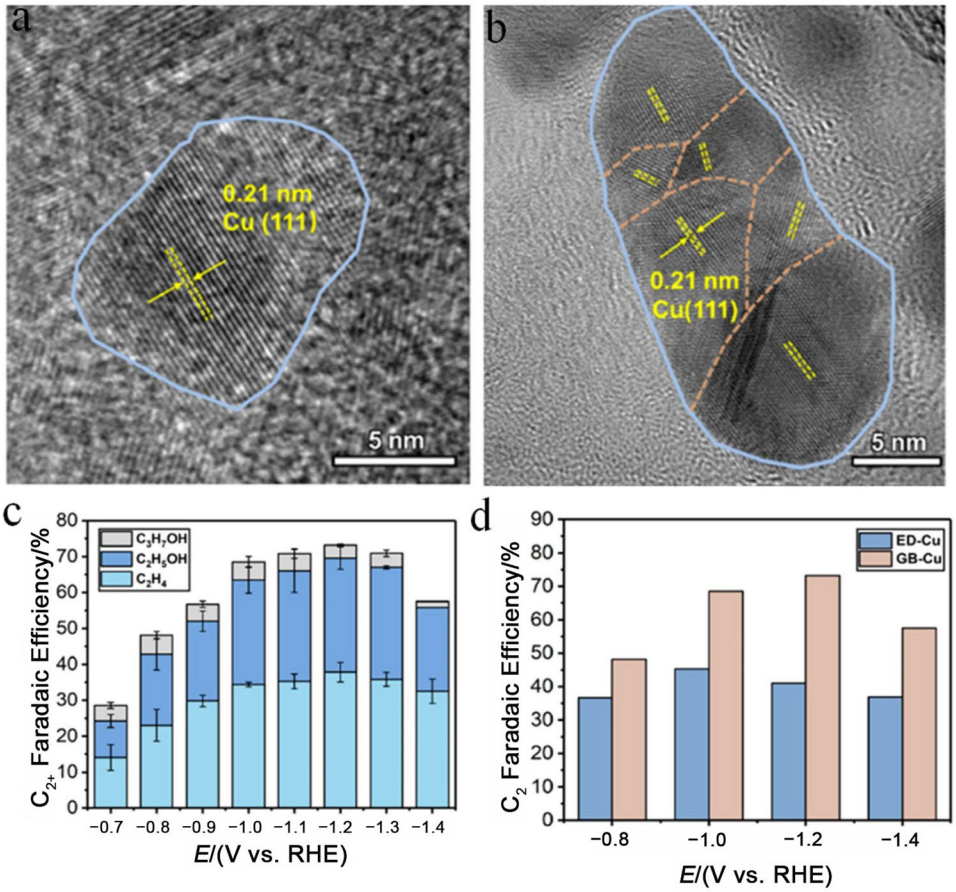

Fig. 12 **a** HR-TEM image of the ED-Cu catalyst; **b** HR-TEM image of the GB-Cu catalyst; **c** FEs for C_{2+} products on GB-Cu; **d** comparison of FEs for C_2 products on ED-Cu and GB-Cu. Reproduced with permission from Ref. [130]. Copyright © 2020, American Chemical Society

of atoms at grain boundaries is irregular, and the atoms at the grain boundaries tend to have higher energy than those within the grains, which can easily be used as active sites to improve the catalytic activity. High-density Cu NW samples were prepared by electrochemical reduction and H_2 reduction (ECR-Cu and HR-Cu, respectively), and the relationship between their CO_2 electrochemical reduction performance and grain boundary density was systematically studied [48, 129]. High-resolution TEM (HR-TEM) results showed that the disordered grain boundaries of Cu NWs gradually decreased with increasing reduction temperature. The electrochemical performance showed that the catalytic activity of the Cu NW electrode was positively correlated with the grain boundary density. In previous studies, the introduction of grain boundaries was usually achieved by reducing CuO, which led to changes in the valence state and morphology of Cu, thus affecting the CO_2 reduction performance. Recently, Gong et al. developed a new method for constructing grain boundaries in Cu electrodes [130]. Polyvinylpyrrolidone was used as an additive to regulate the Cu nucleation kinetics in the electrodeposition process, and then, a Cu electrode (GB-Cu) with abundant grain boundary sites was obtained (Figs. 12a and 12b). Compared with previous studies, this method could construct abundant grain boundaries in Cu catalysts without changing the valence state of copper to better study the influence of grain boundaries on the catalytic performance. The selectivity of GB-Cu for C_2H_4 was higher than that of the ED-Cu electrode without grain boundaries, reaching 38% at −1.2 V versus RHE (Figs. 12c and 12d). In addition, the FE for CO on GB-Cu obviously decreased as the potential became negative, while the FE for C_2H_4 showed a volcano-type trend. The overall selectivity for C_2 products (C_2H_4 and C_2H_5OH) of GB-Cu reached 70% at −1.0 to −1.3 V versus RHE, which was significantly higher than that of ED-Cu, indicating that GB-Cu had better activity for the deep reduction of CO_2. ATR-SEIRAS was used to study the adsorption behavior of CO in the CO_2 electroreduction process and found that the adsorption peak of CO on GB-Cu shifted from 2 070 to 2 060 cm^{-1} at −0.1 V versus RHE, indicating that GB-Cu exhibited stronger adsorption of CO. DFT calculations further verified that the CO binding strength at grain boundary sites (GB1 and GB2) was higher than that at amorphous boundary sites. Therefore, the presence of grain boundaries could promote the adsorption of the key intermediate CO on the Cu surface, thus promoting the C–C coupling reaction to generate C_2 products. Dendritic CuO was synthesized under relatively mild conditions (200–300 °C). The structure was rich in grain boundaries composed of the CuO(110)/CuO(111) facets,

which was conducive to selective generation of ethylene. The FE for ethylene at −1.3 V versus RHE was 78% [131].

In general, the metal surfaces of nanostructures induce the formation of defects and low coordination sites and tightly bind *CO [132] compared with bulk metals, which significantly changes the surface coordination and converts the product from CO to hydrocarbons and alcohols. Ag is also a very promising catalyst for achieving high selectivity in the CO_2RR due to its low overpotential. A porous Ag foam catalyst was studied that had an approximately 60% FE for CH_4 and C_2H_4 at −1.5 V versus RHE [133], which was related to the surface defects and low coordination sites of porous Ag foam. The surface defects and low coordination sites significantly increased the binding energy with CO and resulted in an increase in the FE for CH_4 and C_2H_4. CuO nanosheets were synthesized by the liquid phase method and directly used as CO_2RR electrocatalysts [134]. During the prereduction stage, the CuO nanosheet catalyst underwent dynamic recombination and gradually evolved into coral-like Cu NP aggregates with abundant Cu(100)/Cu(111) grain boundaries. The coral-like structure could limit the retention time of CO and improve the coverage rate of *CO. DFT calculation results showed that the Cu(100)/Cu(111) grain boundaries could reduce the energy barrier of the C–C coupling reaction and promote the generation of C_{2+} products from CO. At a potential of −1.1 V, the FE and current density for a C_{2+} product were 72.1% and 25.2 mA cm^{-2}, respectively. The excellent catalytic performance of the CO_2RR was attributed to the synergistic effect between the coral-like morphology and abundant Cu(100)/Cu(111) grain boundaries. Therefore, combining crystal facet engineering techniques and morphology effects is also an effective way to improve the selectivity for C_{2+} products of Cu-based catalysts. Although the catalytic selectivity of Cu-based catalysts for C_{2+} products could be effectively improved by controlling the crystal facets and morphology, in the actual catalytic process of the CO_2RR, the crystal facets and morphology dynamically change with the electrochemical process, which leads to catalytic selectivity change and even deactivation [135, 136]. Therefore, ensuring the stability of the crystal surface and morphology is the key to practical application of this strategy in the CO_2RR.

4.2 Interface Engineering

The interface of heterogeneous catalysts, especially metal/metal oxide composite catalysts, often has very special electronic characteristics. The unique electronic structure and the synergistic effect between the metal and metal oxide regulate the binding affinity of the intermediate on the catalyst surface and thereby endow the catalysts with improved electrocatalytic activity and selectivity for the CO_2RR. For instance, a low overpotential for the metal site of H_2 was introduced on a metal surface with high H_2 overpotential for interaction between H_2 and CO_2 adsorbed on the adjacent sites, which greatly reduced the overpotential and improved the selectivity in CO_2 reduction. Engineering metal oxide/bimetal interfaces has proven to result in not only superior catalytic activity to the single-component counterparts but also dramatically different catalytic products. In addition, the catalytic stability has also been greatly improved. In recent years, there have been many studies on this aspect [137]. Ag-Cu_2O electrodes were prepared through electrochemical deposition. Ammonia solution (NH_3) and potassium cyanide (KCN) electrolytes were employed to obtain phase-separated Ag-Cu_2O_{PS} and phase-blended Ag-Cu_2O_{PB}, respectively [138]. In the CO_2 electrochemical reduction process, the introduction of Ag inhibited the generation of hydrogen and increased the population of CO, thus regulating the selectivity for ethanol and ethylene. The FE for ethanol was 20.1% and 34.15% on Ag-Cu_2O_{PS} and Ag-Cu_2O_{PB}, respectively, higher than the value of 10.5% for biphase Cu_2O-Cu without Ag doping, which suggested that the optimal interface structure between Ag and Cu was very important and could promote effective transfer of CO from Ag to Cu sites, thus improving the selectivity for ethanol products.

Cu metallic electrodes show great advantages in the electrocatalytic reduction of CO_2. Further modification of the surface can not only prevent poisoning of the electrode itself but also effectively tailor the selectivity for the reduced product. Compared with pure metals, metastable metal oxides on the metal surface can also participate in the electroreduction of CO_2 by stabilizing the CO_2^- intermediate or directly mediating electron transfer, thus significantly improving the catalytic performance in the electrochemical reduction of CO_2. The metal Sn was confirmed to have no catalytic performance in the electroreduction of CO_2, while the oxide SnO_x showed high activity for the CO_2RR [139]. The combination of Sn and SnO_x could produce a synergistic effect, and the composite material had higher performance, which provided new insights to design structures based on Cu catalysts. In situ electrochemical reduction of preformed metal oxides during the reaction to engineer the metal/metal oxide interface is another method to modify metal electrodes toward improved catalytic performance in the electrochemical CO_2RR. Metal oxide catalysts may be partially reduced to the metallic state due to the negative voltage applied to the anode, yielding an "oxide-derived catalyst" [140]. Oxide-derived copper electrodes could convert CO_2 to methanol and improve the selectivity for methanol [141], which was first reported by Fress et al. The deliberate oxidation and reduction of copper catalysts toward an optimal Cu/CuO_x interface structure is crucial to improve the performance in the electrochemical CO_2RR. In addition, the oxide-derived catalysts showed a significant property difference compared with metal catalysts, the reduction of metal oxides in situ on the electrode surface could lead to a change in morphology, and some residual metastable

oxides could change the electronic structure and environment of the active site, thereby tailoring the catalytic behaviors. These metal/metal oxide catalysts could convert CO_2 to not only $2e^-$ reduction reaction products (CO, HCOOH) but also multielectron hydrocarbons (C_2H_4, C_2H_6 and C_2H_5OH). Cu_2O-, CuO- or $Cu(OH)_2$-derived materials are regarded as catalysts with great potential for the electrochemical reduction of CO_2, which can selectively reduce CO_2 at a relatively low potential [142]. Cu_2O is a typical intrinsic p-type semiconductor material with a band gap of 2.1 eV [143]. Thus, growing a layer of Cu_2O on the surface of Cu catalysts through oxidation has attracted increasing attention. A layer of Cu_2O thin film with controllable thickness could be electrodeposited on the surface of a Cu sheet in the copper lactate electrolyte by electrodeposition [47]. The results showed that the thickness of the Cu_2O film had an obvious effect on the selectivity for CO_2 reduction products. When the film thickness was small (the electrodeposition parameter was 3 C cm^{-2}), the reduction product was mainly C_2H_4. When the film thickness was large (the electrodeposition parameter was 11 C cm^{-2}), the reduction product was C_2H_6. In addition, Cu foil was first oxidized in air to form a layer of Cu_2O at 500 °C, and then, a large number of Cu NPs were generated on the surface of Cu foil through electrochemical reduction to obtain a more abundant nanostructure surface and effectively reduce CO_2 [144]. The preparation methods of OD-Cu catalysts can be roughly divided into two categories: annealing methods and nonannealing methods. The preparation method plays a key role in the product distribution. The OD-Cu catalysts prepared by annealing methods had high selectivity for C_1 products (such as CO and formic acid) and low selectivity for C_2 products [48]. In contrast, OD-Cu catalysts prepared by nonannealing methods were more likely to produce C_2 products (such as acetic acid, ethylene and ethanol) [145]. Cu_2O thin films were prepared on polished copper substrates by galvanostatic deposition and converted CO_2 to C_2H_4 and C_2H_5OH products, in which the FEs for C_2H_4 and C_2H_5OH products reached 34%–39% and 9%–16%, respectively, while the formation of CH_4 was significantly inhibited [109]. Metals with rough surfaces have lower coordination sites than metals with smooth surfaces, so they have a larger surface area for electrochemical activity. Therefore, the electrocatalytic performance can be improved by surface treatment of metal. Cu_2O catalysts with different thicknesses (0.2–8.8 μm) were prepared on Cu sheets through constant current deposition and compared with electrolytically polished Cu [146]. These catalysts were used as electrodes for the CO_2RR for 4 200 s, and the surface of the electropolished Cu sheet was still smooth and flat, while the surface of the electrode with deposited Cu_2O was very rough, with Cu NPs of 100 nm or even larger size. The products were analyzed, and the electrode with 3.6 μm thick Cu_2O was found to exhibit the highest selectivity toward the C_2 products. The FEs for ethylene and ethanol were 34.3% and 16.4%, respectively, whereas the FE for methane was less than 1% at −0.99 V versus RHE. In contrast, the FE for ethylene on the electropolished Cu sheet was only 13.8%, and no ethanol could be detected. Cu_2O with a thickness of 3.6 μm was reduced to Cu polyhedral NPs with a thickness of 0.5–1 μm, and the step surface on Cu NPs promoted the formation of C_2 products. In addition, similar results have been reported in the literature [105], in which catalysts derived from Cu_2O showed higher selectivity for C_2 products.

The treatment method of oxide-derived Cu catalysts is particularly important to achieve high selectivity for C_2 products. Surface plasma treatment is one of the most effective methods reported to improve the activity by rapidly changing the chemical state of the surface at room temperature, generating defects and/or removing the capped ligands used for the synthesis of NPs without sintering. Oxygen plasma treatment is another metal preoxidation method. Compared with thermal oxidation, oxygen plasma treatment can quickly change the chemical state on the surface of the catalyst at room temperature, which is more convenient and controllable. Oxygen plasma treatment of metal copper could significantly improve the selectivity for C_2 products [147]. Copper foil was treated with oxygen and hydrogen plasma to prepare novel nanostructured oxide layers and porous surfaces with adjustable morphologies and polycrystalline Cu. Cu_2O-derived Cu NPs with different initial crystal orientations and film thicknesses were studied for the electrochemical CO_2RR, and Cu^+ was found to be the active species for converting CO_2 to ethylene. Using plasma-treated Cu foil as the working electrode, the Cu-Cu_2O catalyst could convert CO_2 to CO, HCOOH and C_2H_4 products at a relatively negative potential, and the FE for C_2H_4 was 60% at −0.9 V versus RHE [109].

In addition, in situ oxidation of the metal electrode during the reaction is also a promising method. For example, a Cu catalyst was oxidized in situ by using a mixture of CO_2/O_2 as the feedstock gas, and in situ oxidation significantly inhibited the generation of CH_4 and improved the selectivity for C_2H_4 [148]. Jim et al. [149] confirmed that metal oxides were involved in CO_2 reduction, and they were regarded as typical zero-dimensional metal catalysts. With the aid of surface and volume induction technology, the Cu_2O electrode was found to be only partially reduced during electrolysis; thus, the product produced by the reduction reaction was the result of the synergistic effect of Cu_2O and Cu. The overpotential of the Cu_2O electrode was only 200 mV. In addition to CO and HCOOH, the Cu catalyst also contributed to the formation of CH_4, while Cu_2O showed better selectivity for C_2H_4. $PdCl_2$ was further introduced into Cu_2O during electrochemical synthesis and improved the selectivity for C_2H_6 [150]. The authors believed that doping of $PdCl_2$ could further activate hydrogen and provide a relatively optimal environment to convert C_2H_4 to C_2H_6. The biphasic electrocatalyst of Cu_2O-Cu was prepared in situ on the surface of a polycrystalline Cu foil,

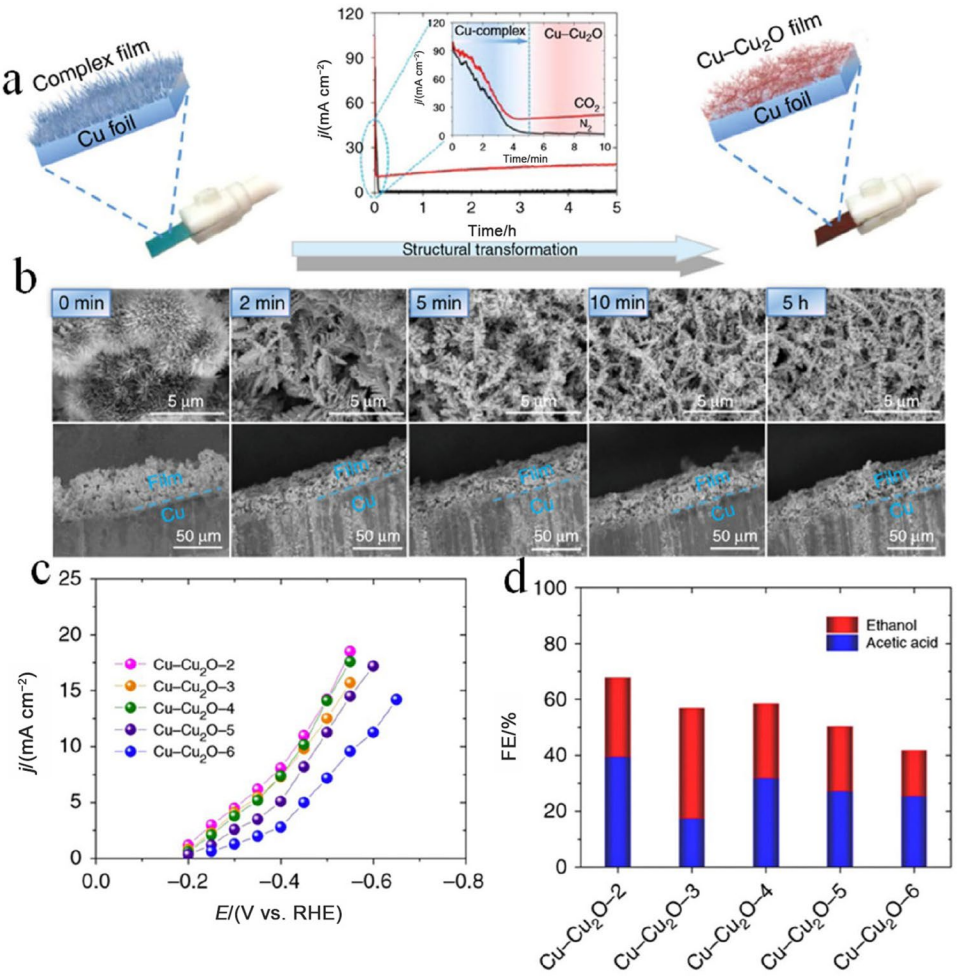

Fig. 13 Decomposition of copper-cuprous oxide electrodes. **a** Reduction current density in 0.1 mol L^{-1} KCl solution saturated with CO_2 and N_2 at an applied potential of −0.4 V versus RHE; the inserts show the current density in the initial stage. **b** SEM images of the electrode with different electroreduction times (0 min, 2 min, 5 min, 10 min, 5 h). **c** Total current density at different applied potentials. **d** FEs for the C_2 products at an applied potential of −0.4 V versus RHE. Reproduced with permission from Ref. [145]. Copyright © 2019, Springer Nature

induced by Cl^- while the electroreduction potential was controlled to be −1.6 V versus RHE, and the FE of the C_2 product could reach 55%. In addition to metal catalysts, various metal oxide catalysts were also loaded onto electrodes to measure the performance for the CO_2RR [151]. A Cu@Cu_2O catalyst was prepared by oxidizing copper rods at room temperature to grow a thin layer of Cu_2O on the surface of Cu rods [152]. The results showed that the Cu@Cu_2O catalyst had excellent selectivity for C_2 (ethylene and ethanol); the FE could reach 50% at −1.0 V versus RHE because Cu_2O on the surface of Cu@Cu_2O was relatively stable during the catalytic process and was not reduced, and the synergistic effect between Cu^+ and Cu^0 on the surface of Cu@Cu_2O was beneficial to improving the selectivity for C_2 products. Figures 13a and 13b show the 3D dendritic Cu-Cu_2O composites obtained by in situ reduction electrodeposition of copper complexes [145], which could efficiently reduce CO_2 to C_2 products (acetic acid and ethanol) at −0.4 V versus RHE. Figures 13c and 13d show that the FE for the C_2 product was up to 80% and that the current density was 11.5 mA cm^{-2}. Subsequent studies showed that the main reason for the excellent catalytic performance of the catalyst for the C_2 product was that the 3D dendritic structure of the catalyst exposed abundant active sites, and the ratio of active sites Cu^+/Cu^0 was appropriate.

By using the wet chemical oxidation process, the oxidation state of copper on the surface of a catalyst can be well controlled to enable the conversion from CO_2 to C_2 products with high FE [153]. For example, a Cu surface was partially oxidized to form an initial Cu(I) chloride layer, which was then converted to a Cu(I) oxide surface. These catalysts were first tested in an H-type electrolytic cell, and the results showed that they had very high C_2 selectivity and that the FE for C_2 products reached 73%. In particular, the FE for C_2H_4 reached 56%, and the total current density was 17 mA cm^{-2}. Then, the catalyst was evaluated by using a flow-type electrolytic cell in a highly alkaline electrolyte. Impressively, it completely suppressed the production of CH_4 and generated a current density of 336 mA cm^{-2}, with a total FE of 84% for C_2 products and a conversion efficiency of 50%. Although oxide-derived metal electrodes have shown excellent catalytic performance in the electrochemical reduction of CO_2, their catalytic mechanism and active sites are still controversial. A study showed that in the electrochemical reduction reaction process, the oxidized copper would be first reduced to metallic copper because the

reduction of copper oxide is more favorable in terms of kinetics and energy than CO_2 reduction [154]. In addition, the stability of residual oxides was explored by using O^{18} isotopes, and the results showed that only a small part of the initial O^{18} remained after the electrochemical CO_2RR (< 1%). Therefore, the excellent catalytic performance of oxide-derived metal electrodes for the CO_2RR was believed to show little relationship with residual oxides [155]. However, many recent studies have identified Cu^0, Cu^+ and their interfaces as the active sites for oxygen-derived copper catalysts [156]. According to theoretical calculations, the presence of Cu^+ and O in the subsurface of the catalyst could promote the activation of CO_2 molecules and the dimerization of the *CO intermediate [157]. Quantum mechanical calculations were used to show that surface Cu^+ species are actually negatively responsible for CO_2 reduction. However, Cu^+ could be partially reduced to Cu^0, and the synergistic effect between Cu^+ and Cu^0 could promote the two key steps of CO_2 adsorption/activation and CO dimerization, which was reflected in both the thermodynamics and kinetics. Specifically, the activation energy barrier of the two steps of CO_2 adsorption/activation and CO dimerization was calculated by comparing three surfaces, namely the pure Cu(111) facet, pure Cu_2O(111) facet and Cu_2O(111) facet partially reduced to Cu^0. The results showed that for the adsorption and activation steps of CO_2, the energy barrier of activation on the surface of pure Cu_2O(111) was the highest, while the energy barrier of activation on the Cu^+/Cu^0 interface was the lowest, and the reaction was exothermic. On the Cu^+/Cu^0 interface, the energy barrier of activation of the endothermic $CO + CO \rightarrow OCCO$ process was even lower than that of the $CO + H \rightarrow CHO$ process, which indicated that the coexisting interface of Cu^+ and Cu^0 increased the ratio of C_2 products to C_1 products. In addition, the product distribution for the CO_2RR could be significantly changed by controlling the oxidation state of Cu [158]. Based on these findings, the design of electrocatalysts that can stabilize the presence of Cu^+ in the reduction reaction will further improve the selectivity for C_{2+} products in the electrochemical reaction of CO_2. By adjusting the oxidation state of Cu, the problem of insufficient catalytic stability caused by unstable factors such as crystal surface and morphology could be effectively overcome [159–162].

4.3 Strong Metal-Support Interactions

In the field of electrocatalysis, metal catalysts are the most widely studied but still have shortcomings, such as low current efficiency and poor stability in the CO_2 reduction process. Catalysts, especially metal nanocatalysts for the CO_2RR, usually undergo agglomeration and exhibit uneven dispersion, which will affect the exposure of active sites and result in decreased accessible active sites. Despite the excellent performance of Cu electrodes in the electrochemical reduction of CO_2, self-supported metal catalysts still present great challenges, and new electrode materials urgently need to be developed. Carbon materials with high specific surface area and electrical conductivity are often used as catalyst supports because they are easy to modify and functionalize. In recent years, carbon supports have been widely used as electrocatalyst supports due to their low cost, large specific surface area and good electrical conductivity. Recombining metals with carbon supports has been proposed as a method to achieve surface modification and improve stability [163–165]. The interface between the support and catalyst can regulate the distribution of electrons for the catalyst, change the adsorption strength of intermediate products and prevent the agglomeration of metal nanocatalysts, thus improving the performance of metal nanocatalysts [166]. Therefore, utilizing the synergistic effect between the support and metal is also one of the strategies to improve the CO_2RR performance. The supports for Cu NCs of foil and carbon paper were compared [167], and Cu NCs deposited on the carbon paper were found to be less stable, in which the size decreased and the surface became rough, even forming a porous structure during the reaction. Therefore, the Cu NCs supported on the carbon paper for the CO_2RR were more inclined to produce methane (the highest FE was approximately 50%), while the highest FE for ethylene was only approximately 25%, which was lower than that of Cu NCs supported on the Cu foil. (The highest FE for ethylene was approximately 50%.)

When a metal is loaded on a heteroatom-doped carbon material, the interaction between the metal and the support can change the electronic structure of the metal, thus improving its intrinsic catalytic activity, which is conducive to the activation of CO_2 molecules and the adjustment of the binding energy of important intermediate products. This is an efficient method to improve the catalytic performance for CO_2. Based on the traditional catalyst system, Cu catalysts were prepared and loaded on various substrates to fully disperse the active NPs and expose the active sites to improve the performance through synergistic effects. The kinetics of CO_2 reduction could be enhanced due to the unique electronic and physical properties of graphene. For example, a variety of carbon materials, including pure graphite (PG), reduced graphene oxide (rGO), GO, nitrogen-doped graphene, carbon nanotubes (CNTs) and carbon gel, were used for deposition of Cu catalysts for electrochemical reduction of CO_2. Cu_2O/rGO composite catalysts were proven to change the selectivity of traditional Cu-based catalysts in the CO_2RR, on which the ethanol production rate was as high as 9.93% [168]. Cu NPs were loaded on the surface of nitrogen-doped multilayer graphene with intense folds and spikes (CNS) to prepare a copper composite catalyst (Cu/CNS) by using electrochemical nucleation. Compared with copper NPs loaded on a GC electrode and Cu NPs not loaded on the surface of CNS, Cu/

CNS composite electrodes for the CO_2RR showed excellent catalytic properties, and the FE for C_2H_5OH at −1.2 V versus RHE was as high as 63%, whereas C_2H_5OH was not detected on the surface of Cu NPs loaded on the GC electrode and Cu NPs not loaded on the surface of CNS. The current densities for C_2H_5OH on the surface of Cu/CNS composite electrodes were 3 times and 5 times higher than those on the surface of copper NPs loaded on the GC electrode and Cu NPs not loaded on the surface of CNS. After 6 h of reaction, the activity and selectivity of the Cu/CNS catalyst did not significantly decrease. Based on electrochemical analysis and DFT calculations, the synergistic effect between Cu NPs and nitrogen-doped carbon plays a key role in the dimerization of the intermediate *CO to C_2H_5OH [169]. In addition, theoretical studies have shown that Cu loaded on graphene improved the catalytic ability and stability because the defect sites could firmly anchor Cu NPs, thus increasing the Cu-graphene interaction. In addition, defect sites would stabilize the reaction intermediates in the CO_2RR process and prevent Cu NPs from agglomerating [170]. Thus, to improve the number of defect sites and the catalytic activity, N-doped graphene was applied as a support to load Cu NPs. Furthermore, carbon lattices doped with N, S or B were explored as supports for Cu NPs, and the neighboring carbon atoms could become the active sites. Cu NPs were assembled on pyridine-rich nitrogen graphene (p-NG) and converted CO_2 to HCOOH at −0.9 V versus RHE and to C_2H_4 at −0.8 V versus RHE with FEs of 62% and 19%, respectively. CO_2 and protons were absorbed by pyridine N functional groups, which effectively promoted the hydrogenation reaction and carbon-carbon coupling reaction and were conducive to generating C_2H_4 products [171]. An Ag-G-NCF composite catalyst was prepared by loading Ag NPs on nitrogen-doped carbon foam wrapped by graphene for the CO_2RR. The FE for C_2H_5OH was up to 82.1%–85.2% at −0.6 to −0.7 V versus RHE, which could react stably for 10 h. However, the current density was approximately as low as 0.31 mA cm^{-2} at −0.5 V versus RHE. The authors believed that the high selectivity for ethanol was due to the ability of pyridine nitrogen to increase the adsorption strength of the intermediate *CO on the surface of the catalyst and promote its conversion to *OC-COH, which finally produced C_2H_5OH [172]. This design would provide a new pathway for the development of non-copper-based electrocatalytic materials that could effectively reduce CO_2 to C_2 products.

In addition to graphene, biomass-based carbon materials have been widely developed in the field of electrochemistry for the CO_2RR due to their high electrical conductivity and strong corrosion resistance. An electrochemical catalyst of monodispersed Cu NPs was prepared by using butterfly wings. The Cu NP/BCF nanocatalyst could convert CO_2 into C_2H_4 with a 67% FE and maintain the stability of the reaction for 24 h [173] because the synergies between pyridine nitrogen and Cu NPs could promote the coupling of C–C bonding and the hydrogenation of intermediate products, and the butterfly wing-derived nitrogen-doped carbon support could effectively prevent Cu NP aggregation. The high catalytic performance of metal composite catalysts mainly came from the synergistic effect between the metal and the support, and optimizing the interaction between the metal and support to adjust the adsorption strength of intermediate products on the surface of the catalyst is essential to improve the catalytic activity and selectivity for the CO_2RR.

4.4 Surface Modification

Surface modification is mainly manifested in the manufacture of surface defects, and its promotion effect on CO_2 electrocatalysis can be summarized from the following aspects: (i) a large number of dangling bonds and unsaturated ligand sites are generated on the surface of nanocatalysts [174], which can be used as the active sites of materials and affect the performance of the CO_2RR by regulating the adsorption strength of different intermediates on the surface of nanocatalysts; (ii) surface defects can regulate the electronic structure of the catalyst, and catalysts rich in defects are usually conducive to charge transfer at the interface [175]. Based on the modification of nanocatalysts, CO_2RR research is mainly focused on the creation of atomic defects (oxygen vacancies, sulfur vacancies or phosphorus vacancies) [176], doping [177], surface etching, etc. [178]. The electronic states and surface structure are important for the selective and active transformation of CO_2. The functionalization strategy on the Cu surface can effectively modify the surface electronic state and chemistry because these functional groups can adjust the adsorption/desorption of reaction intermediates, thus changing the reaction path to form different products. Cu catalysts modified with organic functional groups have good activity and selectivity for the CO_2RR. Cu NPs with a rhombic dodecahedron structure were prepared by modifying Cu NCs with Se-octane as the etching agent [179]. After 12 h of etching, the electrode surface was basically covered by the Cu(110) facet. The experimental results for the CO_2RR showed that the FEs for CH_4 and C_2H_4 reached 58% and 16% at −1.1 V versus Ag/AgCl, respectively. Moreover, compared with the Cu NC structure, the selectivity for CO decreased after etching, and the selectivity for hydrocarbon products significantly improved. Amino acids can also be used to modify copper electrodes for the CO_2RR. The electron-rich groups attached to the exterior of copper can change the adsorption state of CO* on the Cu surface. Cu NWs and Cu foils were modified with different kinds of amino acids, dodecyl mercaptan and stearic acid, respectively [180]. A Cu NW film was synthesized by electrochemically reducing a $Cu(OH)_2$ NW film on Cu foil in $KHCO_3$ solution, and the thickness of the film was estimated to be 0.8 μm. Figure 14a shows a field-emission scanning electron microscopy (FESEM) image of the $Cu(OH)_2$ NW

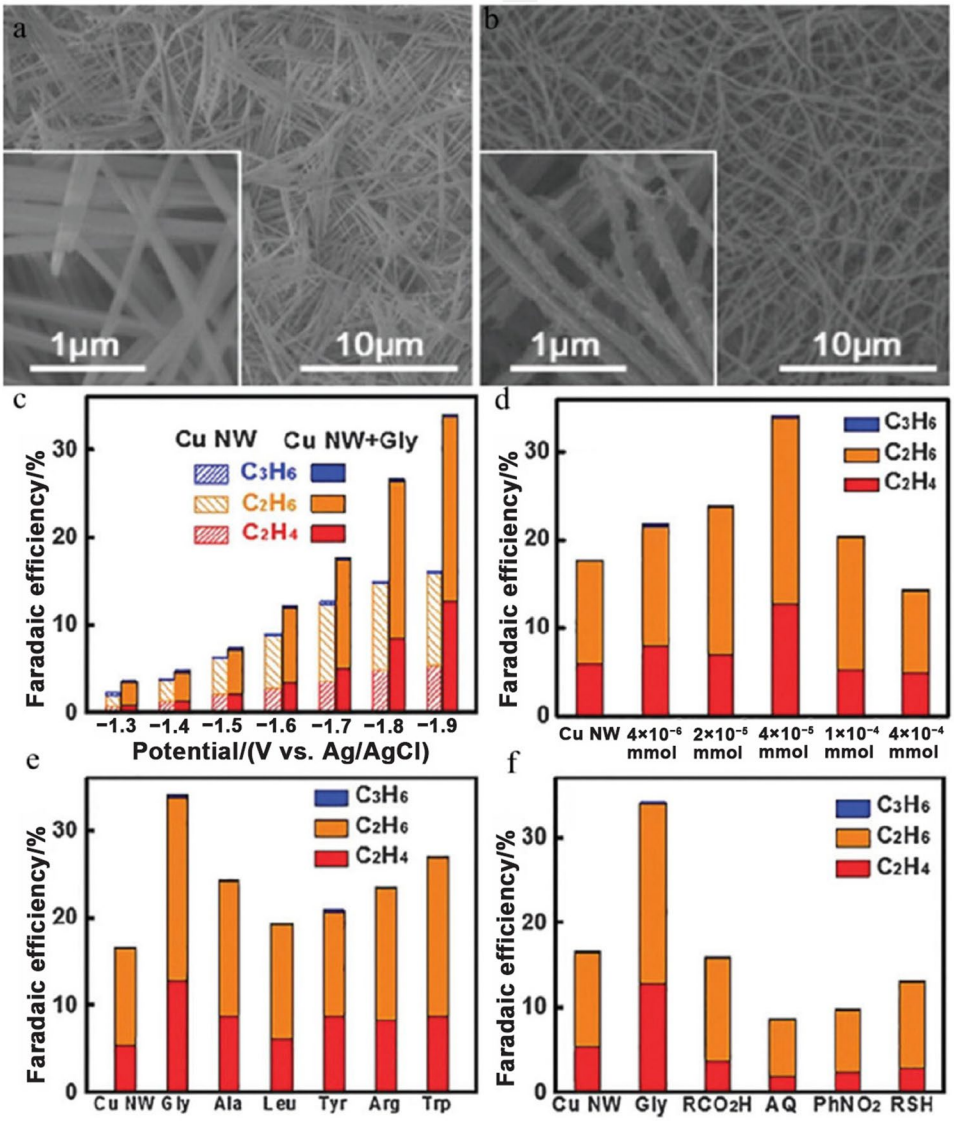

Fig. 14 **a** FESEM image of a $Cu(OH)_2$ NW film. **b** Cu NW film. **c** FE in the full potential range from −1.3 to −1.9 V versus Ag/AgCl. **d** FE for different concentrations of glycine at −1.9 V versus Ag/AgCl. **e** FE with different kinds of amino acids at −1. 9 V versus Ag/AgCl. **f** FE with different kinds of modifiers at −1.9 V versus Ag/AgCl. Reproduced with permission from Ref. [180]. Copyright © 2016, Royal Society of Chemistry

film, which was uniformly coated on the whole surface of the copper foil. FESEM images obtained at higher magnification further revealed that the NWs formed were 100–200 nm in diameter and tens of microns in length (the inset in Fig. 14a). After electrochemical reduction, the Cu NWs still maintained a one-dimensional morphology; however, the straight NWs became curved with the roughened surfaces of the NWs, as shown in Fig. 14b. The FEs for various products obtained on Cu NW films with and without glycine modification are shown in Fig. 14c. The experimental results showed that the FE for C_2H_4 on the surface of Cu NWs treated with glycine reached 34.1% at −1.9 V versus Ag/AgCl, which was significantly higher than that on the untreated electrode (17.8%). To evaluate the effect of the modification degree, the FEs for total hydrocarbons on Cu NW film electrodes with various glycine amounts at a typical potential of −1.9 V versus Ag/AgCl were examined (Fig. 14d). The FEs for total hydrocarbons first increased and then decreased with increasing glycine amount. To clarify which groups affected the selectivity for reduction products in the process of amino acid modification, the electrode was modified by stearic acid (COOH-rich stearic acid) and diazonium salt (NH_2-rich diazonium salt). To determine whether other amino acids would also function in a similar way, various amino acids, including DL-alanine, DL-leucine, DL-tyrosine, DL-arginine and DL-tryptophan, were also investigated, with the same concentration of 1.0 mmol L^{-1}, as shown in Fig. 14e. Cu NW film electrodes modified with all kinds of amino acids performed better in producing hydrocarbons compared with the bare Cu NW film electrode. The Cu nanofilm modified with glycine showed excellent activity for C_2–C_3 hydrocarbons (C_2H_6, C_2H_4 and C_3H_6), with an FE of 34.1%. Figure 14f shows the investigation of other modifiers containing neither –COOH nor $–NH_2$ groups and further confirms the critical role of amino acids in the

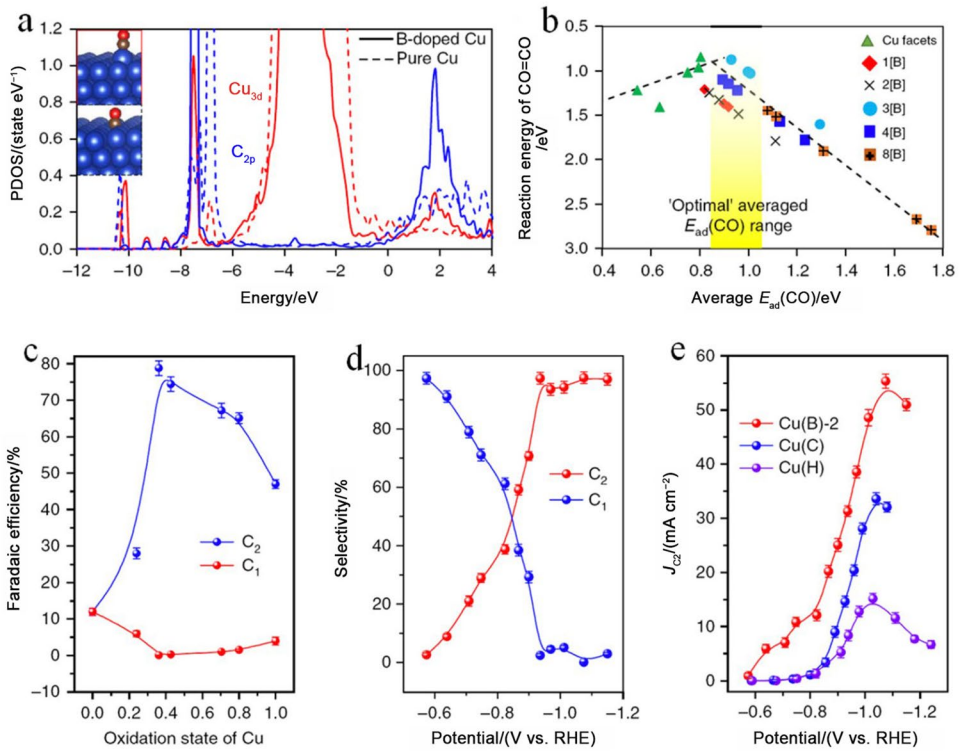

Fig. 15 DFT calculations on enhancing C_2 electroproduction. **a** Partial density of states (PDOS) plot of Cu 3d and C 2p orbitals in pure copper and boron-doped copper catalysts, suggesting that CO has a greater electronic interaction with copper in the Cu(B) system. **b** The CO adsorption energy (E_{ad}) monotonically increases as the partial positive oxidation state of copper increases. **c** FEs for C_2 and C_1 at different copper oxidation states on Cu(B). All samples were tested using the same potential of −1.1 V versus RHE. **d** Conversion efficiencies of reacted CO_2 to C_2 and C_1 products at different potentials on Cu(B)-2. **e** Partial current density of C_2 at different potentials on Cu(B)-2, Cu(C) and Cu(H). Reproduced with permission from Ref. [158]. Copyright © 2018, Springer Nature

promotion of the efficiency of CO_2 conversion to hydrocarbons. The results showed that the C_2H_4 selectivity on the Cu electrode modified with diazonium salt was much higher than that on the electrode modified by stearic acid. Theoretical calculations revealed that hydrogen bond formation between the CHO* and $–NH_3^+$ ends of zwitterionic glycine resulted in extra stabilization of CHO*, which was beneficial to the high activity and selectivity for multicarbon products. MoS_2 was reported to be capable of catalyzing CO_2 to yield C_3H_7OH (approximately 3.5% FE) in 0.1 mol L^{-1} $NaHCO_3$ [181]. The performance of commercial MoS_2 and MoS_2 sputter deposited on silicon thin films for the CO_2RR was investigated, and the FEs for *n*-propanol, ethylene glycol and tert-butanol were only approximately 3.5%, 1% and 1%, respectively. Recently, nickel phosphide (Ni_2P) has demonstrated high selectivity for converting CO_2 to C_3 and C_4 products at overpotentials as low as 10 mV, with an FE for 2,3-furandiol of 71% [182]. These studies have shown that metal carbide, sulfide and phosphide catalysts can convert CO_2 to polycarbonyl alcohols at lower potentials.

The catalytic activity and selectivity of nanocatalysts are closely related to their electronic structure. Doping can change the electronic structure and surface state of catalysts and then tailor the physical structure and electrical conductivity, which greatly improves the catalytic activity for the CO_2RR. A tunable Cu(100) facet was prepared and doped with O and Cl, with variable composition, by using plasma technology to handle Cu foil [183]. Further results confirmed that the presence of O in the surface and subsurface of nanocatalysts was the key to realizing the conversion of CO_2 into hydrocarbons/alcohols, which was even more important than the influence of the Cu(100) facet. The stability of O and the influence on CO binding were explored under reduction conditions through DFT calculations [184]. Researchers first identified the influence of O in the subsurface of nanocatalysts and vacancies on the CO binding energy and then explored the kinetic barrier of O diffusion to the Cu(111) surface, which further proved that O in the subsurface was unstable during the CO_2RR. The stability and diffusion of O in the subsurface of the monocrystalline Cu(111) facet and the Cu(100) facet were studied by DFT [185]. The results showed that O was stabler on the surface than in the subsurface for both crystal directions. The diffusion rate of a single O atom from the bottom of a single Cu layer to the surface was 5×10^3 s^{-1} according to the DFT results, and once proper voltage and dispersion force were applied, CO_2 could be absorbed without subsurface O on the Cu surface. However, accurately simulating the interaction between water molecules and protons in the water reaction process at the current theoretical level was difficult, which hindered further exploration of the electrochemical reduction of CO_2 in aqueous systems. B was used to adjust the ratio of $Cu^{\delta+}$ to Cu^0 active sites to improve the stability and efficiency of electrocatalytic reduction of CO_2 to C_2 products on Cu-based catalysts. The DFT calculation results showed that adjusting the average oxidation state of Cu could control CO adsorption and the C–C dimerization reaction and promote

electrosynthesis of C_2 products. Highly selective C_2 products of the CO_2RR were obtained on boron-doped Cu catalysts with stable electron localization. The relationship between the oxidation state of Cu and the generation of C_2 products by electroreduction of CO_2 has proven theoretically and experimentally, as shown in Figs. 15a and 15b [158]. When the average valence state of Cu was +0.35, a high FE of approximately 80% for C_2 hydrocarbons was achieved. Under these conditions, C_1 and C_3 products were completely inhibited in both the gas and liquid phases (Figs. 15c–15e). The boron-doped Cu catalyst showed excellent stability in producing C_2 from the CO_2RR and maintained high efficiency for nearly 40 h.

5 Conclusion and Outlook

From the perspective of green chemistry and sustainable development strategies, the conversion from carbon dioxide to C_2 or multicarbon products through electrochemical catalysis can effectively alleviate energy shortages and environmental problems. However, the thermodynamic stability and kinetic inertia of CO_2 make it difficult to activate. Therefore, designing and developing efficient catalysts to realize the rapid conversion and utilization of CO_2 is important. This review focuses on electrocatalysts that can catalyze CO_2 reduction to C_2 products. The electrocatalytic CO_2RR is limited by the chemical inertia of CO_2 itself, the low solubility in aqueous solution, and the competition with the HER. Different Cu-based catalysts (e.g., monometallic Cu catalysts, bimetallic catalysts, MOFs, MOF-derived catalysts and other catalysts) and the related reaction mechanisms (carbene dimerization, CO dimerization and CHO + CO coupling) were systematically investigated. Several catalyst strategies, including surface facet engineering, interface engineering, utilization of strong metal-support interactions and surface modification, were proposed to improve the performance in carbon dioxide electrocatalytic reduction. The CO_2RR still faces great challenges in aqueous solutions, and future research should focus on the following directions. (i) In situ characterization techniques and DFT calculations should be developed to gain in-depth insights into the catalytic mechanism for the CO_2RR. The mechanism of the CO_2RR is complex, especially the formation mechanism of C_2 products. Various in situ analysis techniques (in situ XAS, in situ fluorescence spectroscopy, in situ Raman spectroscopy) and DFT calculations are required to capture the intermediate products formed in the CO_2RR process, monitor the dynamic changes on the surface of nanocatalysts and quantitatively analyze the intermediates and products generated in the process of electroreduction, which are necessary to elucidate the mechanism of this complex reaction. (ii) Cocatalysts play a vital role in building a synergistic catalytic system. The composite nanomaterials of main catalysts and cocatalysts could give full play to the good electrical conductivity of metal and the adsorption of small intermediate molecules by the cocatalyst. With the help of cocatalysts, the realization of high-activity, high-stability and even wide-working-potential catalysts is highly promising. The efficient conversion from CO_2 to C_{2+} product fuel could be achieved by building a synergistic catalytic system with a functional organic small molecule-nanometal composite structure. Based on many advantages of small organic molecules as cocatalysts, achievement of efficient conversion from CO_2 to various low-carbon fuels is expected through the construction of a synergistic catalytic system with a functional small organic molecule-nanometal composite structure. (iii) Based on the synergistic effect, SACs show excellent catalytic performance in the electrochemical reaction of CO_2 but still face many problems. To prevent agglomeration, SACs are usually prepared with low metal loading, but their overall activity has difficulty competing with that of NPs, and their selectivity for C_2 products is poor. Therefore, development of new SACs to convert CO_2 into multicarbon products with high activity and high selectivity is essential.

Acknowledgements This work was supported by the Higher Education Discipline Innovation Project (Grant No. D17007), Henan Center for Outstanding Overseas Scientists (Grant No. GZS2022017), National Science Foundation of China (Grant Nos. 21908045, 51922008, 52072114 and 51872075), China Postdoctoral Science Foundation (Grant No. 2018M642754) and Talent Postdoctoral Program for Henan Province (Grant No. ZYQR201810170).

Declarations

Conflict of interest The authors declare no conflict of interest.

References

1. Sanz-Pérez, E.S., Murdock, C.R., Didas, S.A., et al.: Direct capture of CO_2 from ambient air. Chem. Rev. **116**, 11840–11876 (2016). https://doi.org/10.1021/acs.chemrev.6b00173
2. Notz, D., Stroeve, J.: Observed Arctic sea-ice loss directly follows anthropogenic CO_2 emission. Science **354**, 747–750 (2016). https://doi.org/10.1126/science.aag2345
3. Liu, C., Colón, B.C., Ziesack, M., et al.: Water splitting-biosynthetic system with CO_2 reduction efficiencies exceeding photosynthesis. Science **352**, 1210–1213 (2016). https://doi.org/10.1126/science.aaf5039

4. Rockström, J., Gaffney, O., Rogelj, J., et al.: A roadmap for rapid decarbonization. Science **355**, 1269–1271 (2017). https://doi.org/10.1126/science.aah3443
5. Chen, C., Khosrowabadi Kotyk, J.F., Sheehan, S.W.: Progress toward commercial application of electrochemical carbon dioxide reduction. Chem **4**, 2571–2586 (2018). https://doi.org/10.1016/j.chempr.2018.08.019
6. White, J.L., Baruch, M.F., Pander, J.E., et al.: Light-driven heterogeneous reduction of carbon dioxide: photocatalysts and photoelectrodes. Chem. Rev. **115**, 12888–12935 (2015). https://doi.org/10.1021/acs.chemrev.5b00370
7. Gai, P.P., Yu, W., Zhao, H., et al.: Solar-powered organic semiconductor-bacteria biohybrids for CO_2 reduction into acetic acid. Angew. Chem. Int. Ed. **59**, 7224–7229 (2020). https://doi.org/10.1002/anie.202001047
8. Zhang, X.H., Zhang, L., Deng, B.W., et al.: Visible light-responding perovskite oxide catalysts for photo-thermochemical CO_2 reduction. Catal. Commun. **138**, 105955–105960 (2020). https://doi.org/10.1016/j.catcom.2020.105955
9. Tomboc, G.M., Choi, S., Kwon, T., et al.: Potential link between Cu surface and selective CO_2 electroreduction: perspective on future electrocatalyst designs. Adv. Mater. **32**, 1908398 (2020). https://doi.org/10.1002/adma.201908398
10. Kumaravel, V., Bartlett, J., Pillai, S.C.: Photoelectrochemical conversion of carbon dioxide (CO_2) into fuels and value-added products. ACS Energy Lett. **5**, 486–519 (2020). https://doi.org/10.1021/acsenergylett.9b02585
11. Li, D.D., Kassymova, M., Cai, X.C., et al.: Photocatalytic CO_2 reduction over metal-organic framework-based materials. Coord. Chem. Rev. **412**, 213262 (2020). https://doi.org/10.1016/j.ccr.2020.213262
12. Ye, L., Ying, Y.R., Sun, D.R., et al.: Highly efficient porous carbon electrocatalyst with controllable N-species content for selective CO_2 reduction. Angew. Chem. Int. Ed. **59**, 3244–3251 (2020). https://doi.org/10.1002/anie.201912751
13. Choi, W., Kim, M., Kim, B.J., et al.: Electrocatalytic arsenite oxidation in bicarbonate solutions combined with CO_2 reduction to formate. Appl. Catal. B: Environ. **265**, 118607 (2020). https://doi.org/10.1016/j.apcatb.2020.118607
14. Wang, Y.F., Han, P., Lv, X., et al.: Defect and interface engineering for aqueous electrocatalytic CO_2 reduction. Joule **2**, 2551–2582 (2018). https://doi.org/10.1016/j.joule.2018.09.021
15. Zhang, X.Q., Cheng, X.B., Zhang, Q.: Nanostructured energy materials for electrochemical energy conversion and storage: a review. J. Energy Chem. **25**, 967–984 (2016). https://doi.org/10.1016/j.jechem.2016.11.003
16. Yang, H.B., Hung, S.F., Liu, S., et al.: Atomically dispersed Ni(I) as the active site for electrochemical CO_2 reduction. Nat. Energy **3**, 140–147 (2018). https://doi.org/10.1038/s41560-017-0078-8
17. Gao, S., Lin, Y., Jiao, X., et al.: Partially oxidized atomic cobalt layers for carbon dioxide electroreduction to liquid fuel. Nature **529**, 68–71 (2016). https://doi.org/10.1038/nature16455
18. Zhang, Y.J., Sethuraman, V., Michalsky, R., et al.: Competition between CO_2 reduction and H_2 evolution on transition-metal electrocatalysts. ACS Catal. **4**, 3742–3748 (2014). https://doi.org/10.1021/cs5012298
19. Kim, D., Resasco, J., Yu, Y., et al.: Synergistic geometric and electronic effects for electrochemical reduction of carbon dioxide using gold-copper bimetallic nanoparticles. Nat. Commun. **5**, 4948 (2014). https://doi.org/10.1038/ncomms5948
20. Oldham, K.B.: A Gouy-Chapman-Stern model of the double layer at a (metal)/(ionic liquid) interface. J. Electroanal. Chem. **613**, 131–138 (2008). https://doi.org/10.1016/j.jelechem.2007.10.017
21. Li, A., Cao, Q., Zhou, G.Y., et al.: Three-phase photocatalysis for the enhanced selectivity and activity of CO_2 reduction on a hydrophobic surface. Angew. Chem. Int. Ed. **58**, 14549–14555 (2019). https://doi.org/10.1002/anie.201908058
22. Benson, E.E., Kubiak, C.P., Sathrum, A.J., et al.: Electrocatalytic and homogeneous approaches to conversion of CO_2 to liquid fuels. Chem. Soc. Rev. **38**, 89–99 (2009). https://doi.org/10.1039/b804323j
23. Bevilacqua, M., Filippi, J., Miller, H.A., et al.: Recent technological progress in CO_2 electroreduction to fuels and energy carriers in aqueous environments. Energy Technol. **3**, 197–210 (2015). https://doi.org/10.1002/ente.201402166
24. Voiry, D., Yamaguchi, H., Li, J.W., et al.: Enhanced catalytic activity in strained chemically exfoliated WS_2 nanosheets for hydrogen evolution. Nat. Mater. **12**, 850–855 (2013). https://doi.org/10.1038/nmat3700
25. Won, D.H., Shin, H., Koh, J., et al.: Highly efficient, selective, and stable CO_2 electroreduction on a hexagonal Zn catalyst. Angew. Chem. Int. Ed. **55**, 9297–9300 (2016). https://doi.org/10.1002/anie.201602888
26. Bei, J.J., Zhang, R., Chen, Z.D., et al.: Efficient reduction of CO_2 to formate using in situ prepared nano-sized Bi electrocatalyst. Int. J. Electrochem. Sci. (2017). https://doi.org/10.20964/2017.03.72
27. Zhang, B.H., Zhang, J.T.: Rational design of Cu-based electrocatalysts for electrochemical reduction of carbon dioxide. J. Energy Chem. **26**, 1050–1066 (2017). https://doi.org/10.1016/j.jechem.2017.10.011
28. Zhao, Y., Wang, C.Y., Wallace, G.G.: Tin nanoparticles decorated copper oxide nanowires for selective electrochemical reduction of aqueous CO_2 to CO. J. Mater. Chem. A **4**, 10710–10718 (2016). https://doi.org/10.1039/c6ta04155h
29. Ma, S.C., Sadakiyo, M., Heima, M., et al.: Electroreduction of carbon dioxide to hydrocarbons using bimetallic Cu-Pd catalysts with different mixing patterns. J. Am. Chem. Soc. **139**, 47–50 (2017). https://doi.org/10.1021/jacs.6b10740
30. Asadi, M., Kim, K., Liu, C., et al.: Nanostructured transition metal dichalcogenide electrocatalysts for CO_2 reduction in ionic liquid. Science **353**, 467–470 (2016). https://doi.org/10.1126/science.aaf4767
31. Zhang, L., Zhao, Z.J., Gong, J.L.: Nanostructured materials for heterogeneous electrocatalytic CO_2 reduction and their related reaction mechanisms. Angew. Chem. Int. Ed. **56**, 11326–11353 (2017). https://doi.org/10.1002/anie.201612214
32. Zhu, D.D., Liu, J.L., Qiao, S.Z.: Recent advances in inorganic heterogeneous electrocatalysts for reduction of carbon dioxide. Adv. Mater. **28**, 3423–3452 (2016). https://doi.org/10.1002/adma.201504766
33. Park, Y., Lee, Y.W., Kang, S.W., et al.: One-pot synthesis of Au@Pd core-shell nanocrystals with multiple high- and low-index facets and their high electrocatalytic performance. Nanoscale **6**, 9798–9805 (2014). https://doi.org/10.1039/c4nr02034k
34. He, G.N., Zeng, J., Jin, M.S., et al.: A mechanistic study on the nucleation and growth of Au on Pd seeds with a cubic or octahedral shape. ChemCatChem **4**, 1668–1674 (2012). https://doi.org/10.1002/cctc.201200205
35. Gao, D.F., Zhou, H., Wang, J., et al.: Size-dependent electrocatalytic reduction of CO_2 over Pd nanoparticles. J. Am. Chem. Soc. **137**, 4288–4291 (2015). https://doi.org/10.1021/jacs.5b00046
36. Hori, Y., Kikuchi, K., Suzuki, S.: Production of CO and CH_4 in electrochemical reduction of CO_2 at metal electrodes in aqueous hydrogencarbonate solution. Chem. Lett. **14**, 1695–1698 (1985). https://doi.org/10.1246/cl.1985.1695
37. Hori, Y., Kikuchi, K., Murata, A., et al.: Production of methane and ethylene in electrochemical reduction of carbon dioxide at copper electrode in aqueous hydrogencarbonate solution. Chem. Lett. **15**, 897–898 (1986). https://doi.org/10.1246/cl.1986.897

38. Hori, Y., Murata, A., Takahashi, R., et al.: Electroreduction of CO to CH_4 and C_2H_4 at a copper electrode in aqueous solutions at ambient temperature and pressure. J. Am. Chem. Soc. **109**, 5022–5023 (1987). https://doi.org/10.1021/ja00250a044
39. Hori, Y., Murata, A., Takahashi, R.: Formation of hydrocarbons in the electrochemical reduction of carbon dioxide at a copper electrode in aqueous solution. J. Chem. Soc. Faraday Trans. **85**, 2309–2326 (1989). https://doi.org/10.1039/f19898502309
40. Kuhl, K.P., Cave, E.R., Abram, D.N., et al.: New insights into the electrochemical reduction of carbon dioxide on metallic copper surfaces. Energy Environ. Sci. **5**, 7050–7059 (2012). https://doi.org/10.1039/c2ee21234j
41. Kuhl, K.P., Hatsukade, T., Cave, E.R., et al.: Electrocatalytic conversion of carbon dioxide to methane and methanol on transition metal surfaces. J. Am. Chem. Soc. **136**, 14107–14113 (2014). https://doi.org/10.1021/ja505791r
42. Sen, S., Liu, D., Palmore, G.T.R.: Electrochemical reduction of CO_2 at copper nanofoams. ACS Catal. **4**, 3091–3095 (2014). https://doi.org/10.1021/cs500522g
43. Lum, Y., Kwon, Y., Lobaccaro, P., et al.: Trace levels of copper in carbon materials show significant electrochemical CO_2 reduction activity. ACS Catal. **6**, 202–209 (2016). https://doi.org/10.1021/acscatal.5b02399
44. Ma, W.C., Xie, S.J., Zhang, X.G., et al.: Promoting electrocatalytic CO_2 reduction to formate via sulfur-boosting water activation on indium surfaces. Nat. Commun. **10**, 892 (2019). https://doi.org/10.1038/s41467-019-08805-x
45. Dou, S., Song, J.J., Xi, S.B., et al.: Boosting electrochemical CO_2 reduction on metal-organic frameworks via ligand doping. Angew. Chem. Int. Ed. **58**, 4041–4045 (2019). https://doi.org/10.1002/anie.201814711
46. Cao, Z., Zacate, S.B., Sun, X.D., et al.: Tuning gold nanoparticles with chelating ligands for highly efficient electrocatalytic CO_2 reduction. Angew. Chem. Int. Ed. **57**, 12675–12679 (2018). https://doi.org/10.1002/anie.201805696
47. Kas, R., Kortlever, R., Milbrat, A., et al.: Electrochemical CO_2 reduction on Cu_2O-derived copper nanoparticles: controlling the catalytic selectivity of hydrocarbons. Phys. Chem. Chem. Phys. **16**, 12194–12201 (2014). https://doi.org/10.1039/c4cp01520g
48. Raciti, D., Livi, K.J., Wang, C.: Highly dense Cu nanowires for low-overpotential CO_2 reduction. Nano Lett **15**, 6829–6835 (2015). https://doi.org/10.1021/acs.nanolett.5b03298
49. Li, Y.F., Cui, F., Ross, M.B., et al.: Structure-sensitive CO_2 electroreduction to hydrocarbons on ultrathin 5-fold twinned copper nanowires. Nano Lett. **17**, 1312–1317 (2017). https://doi.org/10.1021/acs.nanolett.6b05287
50. Dutta, A., Rahaman, M., Luedi, N.C., et al.: Morphology matters: tuning the product distribution of CO_2 electroreduction on oxide-derived Cu foam catalysts. ACS Catal. **6**, 3804–3814 (2016). https://doi.org/10.1021/acscatal.6b00770
51. Reske, R., Mistry, H., Behafarid, F., et al.: Particle size effects in the catalytic electroreduction of CO_2 on Cu nanoparticles. J. Am. Chem. Soc. **136**, 6978–6986 (2014). https://doi.org/10.1021/ja500328k
52. Merino-Garcia, I., Albo, J., Irabien, A.: Tailoring gas-phase CO_2 electroreduction selectivity to hydrocarbons at Cu nanoparticles. Nanotechnology **29**, 014001 (2018). https://doi.org/10.1088/1361-6528/aa994e
53. Loiudice, A., Lobaccaro, P., Kamali, E.A., et al.: Tailoring copper nanocrystals towards C_2 products in electrochemical CO_2 reduction. Angew. Chem. Int. Ed. **55**, 5789–5792 (2016). https://doi.org/10.1002/anie.201601582
54. Kim, D., Kley, C.S., Li, Y.F., et al.: Copper nanoparticle ensembles for selective electroreduction of CO_2 to C_2–C_3 products. PNAS **114**, 10560–10565 (2017). https://doi.org/10.1073/pnas.1711493114
55. Wang, X.L., Varela, A.S., Bergmann, A., et al.: Catalyst particle density controls hydrocarbon product selectivity in CO_2 electroreduction on CuO_x. Chemsuschem **10**, 4642–4649 (2017). https://doi.org/10.1002/cssc.201701179
56. Tang, W., Peterson, A.A., Varela, A.S., et al.: The importance of surface morphology in controlling the selectivity of polycrystalline copper for CO_2 electroreduction. Phys. Chem. Chem. Phys. **14**, 76–81 (2012). https://doi.org/10.1039/c1cp22700a
57. Mi, Y., Shen, S., Peng, X., et al.: Selective electroreduction of CO_2 to C_2 products over Cu_3N-derived Cu nanowires. ChemElectroChem **6**, 2393–2397 (2019). https://doi.org/10.1002/celc.201801826
58. Nur Hossain, M., Chen, S., Chen, A.C.: Thermal-assisted synthesis of unique Cu nanodendrites for the efficient electrochemical reduction of CO_2. Appl. Catal. B: Environ. **259**, 118096 (2019). https://doi.org/10.1016/j.apcatb.2019.118096
59. Ye, K., Cao, A., Shao, J.Q., et al.: Synergy effects on Sn-Cu alloy catalyst for efficient CO_2 electroreduction to formate with high mass activity. Sci. Bull. **65**, 711–719 (2020). https://doi.org/10.1016/j.scib.2020.01.020
60. Kim, D., Xie, C.L., Becknell, N., et al.: Electrochemical activation of CO_2 through atomic ordering transformations of AuCu nanoparticles. J. Am. Chem. Soc. **139**, 8329–8336 (2017). https://doi.org/10.1021/jacs.7b03516
61. Ren, D., Ang, B.S.H., Yeo, B.S.: Tuning the selectivity of carbon dioxide electroreduction toward ethanol on oxide-derived Cu_xZn catalysts. ACS Catal. **6**, 8239–8247 (2016). https://doi.org/10.1021/acscatal.6b02162
62. Ishimaru, S., Shiratsuchi, R., Nogami, G.: Pulsed electroreduction of CO_2 on Cu-Ag alloy electrodes. J. Electrochem. Soc. **147**, 1864–1867 (2000). https://doi.org/10.1149/1.1393448
63. Jia, F.L., Yu, X.X., Zhang, L.Z.: Enhanced selectivity for the electrochemical reduction of CO_2 to alcohols in aqueous solution with nanostructured Cu-Ag alloy as catalyst. J. Power Sources **252**, 85–89 (2014). https://doi.org/10.1016/j.jpowsour.2013.12.002
64. Bligaard, T., Nørskov, J.K.: Ligand effects in heterogeneous catalysis and electrochemistry. Electrochim. Acta **52**, 5512–5516 (2007). https://doi.org/10.1016/j.electacta.2007.02.041
65. Clark, E.L., Hahn, C., Jaramillo, T.F., et al.: Electrochemical CO_2 reduction over compressively strained CuAg surface alloys with enhanced multi-carbon oxygenate selectivity. J. Am. Chem. Soc. **139**, 15848–15857 (2017). https://doi.org/10.1021/jacs.7b08607
66. Hoang, T.T.H., Verma, S., Ma, S.C., et al.: Nanoporous copper-silver alloys by additive-controlled electrodeposition for the selective electroreduction of CO_2 to ethylene and ethanol. J. Am. Chem. Soc. **140**, 5791–5797 (2018). https://doi.org/10.1021/jacs.8b01868
67. Kortlever, R., Peters, I., Balemans, C., et al.: Palladium-gold catalyst for the electrochemical reduction of CO_2 to C_1–C_5 hydrocarbons. Chem. Commun. **52**, 10229–10232 (2016). https://doi.org/10.1039/c6cc03717h
68. Torelli, D.A., Francis, S.A., Crompton, J.C., et al.: Nickel-gallium-catalyzed electrochemical reduction of CO_2 to highly reduced products at low overpotentials. ACS Catal. **6**, 2100–2104 (2016). https://doi.org/10.1021/acscatal.5b02888
69. Paris, A.R., Bocarsly, A.B.: Ni-Al films on glassy carbon electrodes generate an array of oxygenated organics from CO_2. ACS Catal. **7**, 6815–6820 (2017). https://doi.org/10.1021/acscatal.7b02146
70. Wang, Q.C., Lei, Y.P., Wang, D.S., et al.: Defect engineering in earth-abundant electrocatalysts for CO_2 and N_2 reduction. Energy Environ. Sci. **12**, 1730–1750 (2019). https://doi.org/10.1039/c8ee03781g
71. Diercks, C.S., Liu, Y.Z., Cordova, K.E., et al.: The role of reticular chemistry in the design of CO_2 reduction catalysts. Nat. Mater. **17**, 301–307 (2018). https://doi.org/10.1038/s41563-018-0033-5

72. He, H.M., Perman, J.A., Zhu, G.S., et al.: Metal-organic frameworks for CO_2 chemical transformations. Small **12**, 6309–6324 (2016). https://doi.org/10.1002/smll.201602711
73. Wang, J.W., Huang, H.H., Sun, J.K., et al.: Syngas production with a highly-robust nickel(II) homogeneous electrocatalyst in a water-containing system. ACS Catal. **8**, 7612–7620 (2018). https://doi.org/10.1021/acscatal.8b02044
74. Weng, Z., Wu, Y.S., Wang, M.Y., et al.: Active sites of copper-complex catalytic materials for electrochemical carbon dioxide reduction. Nat. Commun. **9**, 415 (2018). https://doi.org/10.1038/s41467-018-02819-7
75. Yang, Q., Xu, Q., Jiang, H.L.: Metal-organic frameworks meet metal nanoparticles: synergistic effect for enhanced catalysis. Chem Soc Rev **46**, 4774–4808 (2017). https://doi.org/10.1039/c6cs00724d
76. Yang, F., Chen, A.L., Deng, P.L., et al.: Highly efficient electroconversion of carbon dioxide into hydrocarbons by cathodized copper-organic frameworks. Chem. Sci. **10**, 7975–7981 (2019). https://doi.org/10.1039/c9sc02605c
77. Nam, D.H., Bushuyev, O.S., Li, J., et al.: Metal-organic frameworks mediate Cu coordination for selective CO_2 electroreduction. J. Am. Chem. Soc. **140**, 11378–11386 (2018). https://doi.org/10.1021/jacs.8b06407
78. Senthil Kumar, R., Senthil Kumar, S., Anbu Kulandainathan, M.: Highly selective electrochemical reduction of carbon dioxide using Cu based metal organic framework as an electrocatalyst. Electrochem. Commun. **25**, 70–73 (2012). https://doi.org/10.1016/j.elecom.2012.09.018
79. Li, J.R., Kuppler, R.J., Zhou, H.C.: Selective gas adsorption and separation in metal-organic frameworks. Chem. Soc. Rev. **38**, 1477–1504 (2009). https://doi.org/10.1039/b802426j
80. Cheng, Y.S., Chu, X.P., Ling, M., et al.: An MOF-derived copper@nitrogen-doped carbon composite: the synergistic effects of N-types and copper on selective CO_2 electroreduction. Catal. Sci. Technol. **9**, 5668–5675 (2019). https://doi.org/10.1039/c9cy01131e
81. Zhao, K., Liu, Y.M., Quan, X., et al.: CO_2 electroreduction at low overpotential on oxide-derived Cu/carbons fabricated from metal organic framework. ACS Appl. Mater. Interfaces **9**, 5302–5311 (2017). https://doi.org/10.1021/acsami.6b15402
82. Ge, L., Wang, L., Rudolph, V., et al.: Hierarchically structured metal-organic framework/vertically-aligned carbon nanotubes hybrids for CO_2 capture. RSC Adv. **3**, 25360 (2013). https://doi.org/10.1039/c3ra44250k
83. Aguilera-Sigalat, J., Bradshaw, D.: Synthesis and applications of metal-organic framework-quantum dot (QD@MOF) composites. Coord. Chem. Rev. **307**, 267–291 (2016). https://doi.org/10.1016/j.ccr.2015.08.004
84. Rong, X., Wang, H.J., Lu, X.L., et al.: Controlled synthesis of a vacancy-defect single-atom catalyst for boosting CO_2 electroreduction. Angew. Chem. Int. Ed. **59**, 1961–1965 (2020). https://doi.org/10.1002/anie.201912458
85. Yang, H.P., Wu, Y., Li, G.D., et al.: Scalable production of efficient single-atom copper decorated carbon membranes for CO_2 electroreduction to methanol. J. Am. Chem. Soc. **141**, 12717–12723 (2019). https://doi.org/10.1021/jacs.9b04907
86. Fei, H.L., Dong, J.C., Wan, C.Z., et al.: Microwave-assisted rapid synthesis of graphene-supported single atomic metals. Adv. Mater. **30**, 1802146 (2018). https://doi.org/10.1002/adma.201802146
87. Ye, S.H., Luo, F.Y., Zhang, Q.L., et al.: Highly stable single Pt atomic sites anchored on aniline-stacked graphene for hydrogen evolution reaction. Energy Environ. Sci. **12**, 1000–1007 (2019). https://doi.org/10.1039/c8ee02888e
88. Wang, Y.F., Chen, Z., Han, P., et al.: Single-atomic Cu with multiple oxygen vacancies on ceria for electrocatalytic CO_2 reduction to CH_4. ACS Catal. **8**, 7113–7119 (2018). https://doi.org/10.1021/acscatal.8b01014
89. Qiao, B.T., Wang, A.Q., Yang, X.F., et al.: Single-atom catalysis of CO oxidation using Pt_1/FeO_x. Nat. Chem. **3**, 634–641 (2011). https://doi.org/10.1038/nchem.1095
90. Zhu, C.Z., Fu, S.F., Shi, Q.R., et al.: Single-atom electrocatalysts. Angew. Chem. Int. Ed. **56**, 13944–13960 (2017). https://doi.org/10.1002/anie.201703864
91. Back, S., Jung, Y.: TiC- and TiN-supported single-atom catalysts for dramatic improvements in CO_2 electrochemical reduction to CH_4. ACS Energy Lett. **2**, 969–975 (2017). https://doi.org/10.1021/acsenergylett.7b00152
92. Cheng, M.J., Clark, E.L., Pham, H.H., et al.: Quantum mechanical screening of single-atom bimetallic alloys for the selective reduction of CO_2 to C_1 hydrocarbons. ACS Catal. **6**, 7769–7777 (2016). https://doi.org/10.1021/acscatal.6b01393
93. Back, S., Lim, J., Kim, N.Y., et al.: Single-atom catalysts for CO_2 electroreduction with significant activity and selectivity improvements. Chem. Sci. **8**, 1090–1096 (2017). https://doi.org/10.1039/c6sc03911a
94. Ju, W., Bagger, A., Hao, G.P., et al.: Understanding activity and selectivity of metal-nitrogen-doped carbon catalysts for electrochemical reduction of CO_2. Nat. Commun. **8**, 944–953 (2017). https://doi.org/10.1038/s41467-017-01035-z
95. Yang, F., Song, P., Liu, X.Z., et al.: Highly efficient CO_2 electroreduction on ZnN_4-based single-atom catalyst. Angew. Chem. Int. Ed. **57**, 12303–12307 (2018). https://doi.org/10.1002/anie.201805871
96. Zheng, T.T., Jiang, K., Ta, N., et al.: Large-scale and highly selective CO_2 electrocatalytic reduction on nickel single-atom catalyst. Joule **3**, 265–278 (2019). https://doi.org/10.1016/j.joule.2018.10.015
97. Gu, J., Hsu, C.S., Bai, L., et al.: Atomically dispersed Fe^{3+} sites catalyze efficient CO_2 electroreduction to CO. Science **364**, 1091–1094 (2019). https://doi.org/10.1126/science.aaw7515
98. Lu, X.L., Rong, X., Zhang, C., et al.: Carbon-based single-atom catalysts for CO_2 electroreduction: progress and optimization strategies. J. Mater. Chem. A **8**, 10695–10708 (2020). https://doi.org/10.1039/d0ta01955k
99. Xiang, K.S., Liu, Y.C., Yu, H., et al.: Strategies to improve the performance of copper-based catalyst for electroreduction of CO_2 to multi-carbon products. Chin. Sci. Bull. **65**, 3360–3372 (2020). https://doi.org/10.1360/tb-2020-0014
100. Jiao, Y., Zheng, Y., Chen, P., et al.: Molecular scaffolding strategy with synergistic active centers to facilitate electrocatalytic CO_2 reduction to hydrocarbon/alcohol. J. Am. Chem. Soc. **139**, 18093–18100 (2017). https://doi.org/10.1021/jacs.7b10817
101. Cheng, S.A., Xing, D.F., Call, D.F., et al.: Direct biological conversion of electrical current into methane by electromet hanogenesis. Environ. Sci. Technol. **43**, 3953–3958 (2009). https://doi.org/10.1021/es803531g
102. Liu, Y.M., Chen, S., Quan, X., et al.: Efficient electrochemical reduction of carbon dioxide to acetate on nitrogen-doped nanodiamond. J. Am. Chem. Soc. **137**, 11631–11636 (2015). https://doi.org/10.1021/jacs.5b02975
103. Wu, J.J., Ma, S.C., Sun, J., et al.: A metal-free electrocatalyst for carbon dioxide reduction to multi-carbon hydrocarbons and oxygenates. Nat. Commun. **7**, 13869–13875 (2016). https://doi.org/10.1038/ncomms13869
104. Liu, Y.M., Zhang, Y.J., Cheng, K., et al.: Selective electrochemical reduction of carbon dioxide to ethanol on a boron- and nitrogen-co-doped nanodiamond. Angew. Chem. Int. Ed. **56**, 15607–15611 (2017). https://doi.org/10.1002/anie.201706311
105. Mistry, H., Varela, A.S., Bonifacio, C.S., et al.: Highly selective plasma-activated copper catalysts for carbon dioxide reduction to

ethylene. Nat. Commun. **7**, 12123 (2016). https://doi.org/10.1038/ncomms12123
106. Angamuthu, R., Byers, P., Lutz, M., et al.: Electrocatalytic CO_2 conversion to oxalate by a copper complex. Science **327**, 313–315 (2010). https://doi.org/10.1126/science.1177981
107. Gattrell, M., Gupta, N., Co, A.: A review of the aqueous electrochemical reduction of CO_2 to hydrocarbons at copper. J. Electroanal. Chem. **594**, 1–19 (2006). https://doi.org/10.1016/j.jelechem.2006.05.013
108. Nie, X.W., Esopi, M.R., Janik, M.J., et al.: Selectivity of CO_2 reduction on copper electrodes: the role of the kinetics of elementary steps. Angew. Chem. Int. Ed. **52**, 2459–2462 (2013). https://doi.org/10.1002/anie.201208320
109. Kas, R., Kortlever, R., Yılmaz, H., et al.: Manipulating the hydrocarbon selectivity of copper nanoparticles in CO_2 electroreduction by process conditions. ChemElectroChem **2**, 354–358 (2015). https://doi.org/10.1002/celc.201402373
110. DeWulf, D.W., Jin, T., Bard, A.J.: Electrochemical and surface studies of carbon dioxide reduction to methane and ethylene at copper electrodes in aqueous solutions. J. Electrochem. Soc. **136**, 1686–1691 (1989). https://doi.org/10.1149/1.2096993
111. Calle-Vallejo, F., Koper, M.T.M.: Theoretical considerations on the electroreduction of CO to C_2 species on Cu(100) electrodes. Angew. Chem. Int. Ed. **52**, 7282–7285 (2013). https://doi.org/10.1002/anie.201301470
112. Pérez-Gallent, E., Figueiredo, M.C., Calle-Vallejo, F., et al.: Spectroscopic observation of a hydrogenated CO dimer intermediate during CO reduction on Cu(100) electrodes. Angew. Chem. Int. Ed. **56**, 3621–3624 (2017). https://doi.org/10.1002/anie.201700580
113. Montoya, J.H., Shi, C., Chan, K.R., et al.: Theoretical insights into a CO dimerization mechanism in CO_2 electroreduction. J. Phys. Chem. Lett. **6**, 2032–2037 (2015). https://doi.org/10.1021/acs.jpclett.5b00722
114. Montoya, J.H., Peterson, A.A., Nørskov, J.K.: Insights into C-C coupling in CO_2 electroreduction on copper electrodes. ChemCatChem **5**, 737–742 (2013). https://doi.org/10.1002/cctc.201200564
115. Hunter, B.M., Gray, H.B., Müller, A.M.: Earth-abundant heterogeneous water oxidation catalysts. Chem Rev **116**, 14120–14136 (2016). https://doi.org/10.1021/acs.chemrev.6b00398
116. Dongfang, C., Zhao, Z.J., Zhang, G., et al.: The nature of active sites for carbon dioxide electroreduction over oxide-derived copper catalysts. Nat. Commun. **12**, 395 (2021). https://doi.org/10.1038/s41467-020-20615-0
117. Schouten, K.J.P., Kwon, Y., van der Ham, C.J.M., et al.: A new mechanism for the selectivity to C_1 and C_2 species in the electrochemical reduction of carbon dioxide on copper electrodes. Chem. Sci. **2**, 1902–1909 (2011). https://doi.org/10.1039/c1sc00277e
118. Luo, W.J., Nie, X.W., Janik, M.J., et al.: Facet dependence of CO_2 reduction paths on Cu electrodes. ACS Catal. **6**, 219–229 (2016). https://doi.org/10.1021/acscatal.5b01967
119. Garza, A.J., Bell, A.T., Head-Gordon, M.: Mechanism of CO_2 reduction at copper surfaces: pathways to C_2 products. ACS Catal. **8**, 1490–1499 (2018). https://doi.org/10.1021/acscatal.7b03477
120. Ma, W.C., Xie, S.J., Liu, T.T., et al.: Electrocatalytic reduction of CO_2 to ethylene and ethanol through hydrogen-assisted C–C coupling over fluorine-modified copper. Nat. Catal. **3**, 478–487 (2020). https://doi.org/10.1038/s41929-020-0450-0
121. He, R., Wang, Y.C., Wang, X.Y., et al.: Facile synthesis of pentacle gold-copper alloy nanocrystals and their plasmonic and catalytic properties. Nat. Commun. **5**, 4327 (2014). https://doi.org/10.1038/ncomms5327
122. Hori, Y., Takahashi, I., Koga, O., et al.: Electrochemical reduction of carbon dioxide at various series of copper single crystal electrodes. J. Mol. Catal. A: Chem. **199**, 39–47 (2003). https://doi.org/10.1016/S1381-1169(03)00016-5
123. Schouten, K.J.P., Qin, Z.S., Pérez Gallent, E., et al.: Two pathways for the formation of ethylene in CO reduction on single-crystal copper electrodes. J. Am. Chem. Soc. **134**, 9864–9867 (2012). https://doi.org/10.1021/ja302668n
124. Kim, Y.G., Javier, A., Baricuatro, J.H., et al.: Regulating the product distribution of CO reduction by the atomic-level structural modification of the Cu electrode surface. Electrocatalysis **7**, 391–399 (2016). https://doi.org/10.1007/s12678-016-0314-1
125. Durand, W.J., Peterson, A.A., Studt, F., et al.: Structure effects on the energetics of the electrochemical reduction of CO_2 by copper surfaces. Surf. Sci. **605**, 1354–1359 (2011). https://doi.org/10.1016/j.susc.2011.04.028
126. Chen, C.S., Handoko, A.D., Wan, J.H., et al.: Stable and selective electrochemical reduction of carbon dioxide to ethylene on copper mesocrystals. Catal. Sci. Technol. **5**, 161–168 (2015). https://doi.org/10.1039/c4cy00906a
127. Roberts, F.S., Kuhl, K.P., Nilsson, A.: High selectivity for ethylene from carbon dioxide reduction over copper nanocube electrocatalysts. Angew. Chem. Int. Ed. **54**, 5179–5182 (2015). https://doi.org/10.1002/anie.201412214
128. Zhong, D.Z., Zhao, Z.J., Zhao, Q., et al.: Coupling of Cu(100) and (110) facets promotes carbon dioxide conversion to hydrocarbons and alcohols. Angew. Chem. Int. Ed. **60**, 4879–4885 (2021). https://doi.org/10.1002/anie.202015159
129. Cao, L., Raciti, D., Li, C.Y., et al.: Mechanistic insights for low-overpotential electroreduction of CO_2 to CO on copper nanowires. ACS Catal. **7**, 8578–8587 (2017). https://doi.org/10.1021/acscatal.7b03107
130. Chen, Z.Q., Wang, T., Liu, B., et al.: Grain-boundary-rich copper for efficient solar-driven electrochemical CO_2 reduction to ethylene and ethanol. J. Am. Chem. Soc. **142**, 6878–6883 (2020). https://doi.org/10.1021/jacs.0c00971
131. Tan, Z.H., Peng, T.Y., Tan, X.J., et al.: Controllable synthesis of leaf-like CuO nanosheets for selective CO_2 electroreduction to ethylene. ChemElectroChem **7**, 2020–2025 (2020). https://doi.org/10.1002/celc.202000235
132. Verdaguer-Casadevall, A., Li, C.W., Johansson, T.P., et al.: Probing the active surface sites for CO reduction on oxide-derived copper electrocatalysts. J. Am. Chem. Soc. **137**, 9808–9811 (2015). https://doi.org/10.1021/jacs.5b06227
133. Dutta, A., Morstein, C.E., Rahaman, M., et al.: Beyond copper in CO_2 electrolysis: effective hydrocarbon production on silver-nanofoam catalysts. ACS Catal. **8**, 8357–8368 (2018). https://doi.org/10.1021/acscatal.8b01738
134. Xu, Z., Wu, T.C., Cao, Y., et al.: Dynamic restructuring induced Cu nanoparticles with ideal nanostructure for selective multicarbon compounds production via carbon dioxide electroreduction. J. Catal. **383**, 42–50 (2020). https://doi.org/10.1016/j.jcat.2020.01.002
135. Kim, Y.G., Baricuatro, J.H., Javier, A., et al.: The evolution of the polycrystalline copper surface, first to Cu(111) and then to Cu(100), at a fixed CO_2RR potential: a study by operando EC-STM. Langmuir **30**, 15053–15056 (2014). https://doi.org/10.1021/la504445g
136. Liu, H., Xiang, K.S., Liu, Y.C., et al.: Polydopamine functionalized Cu nanowires for enhanced CO_2 electroreduction towards methane. ChemElectroChem **5**, 3991–3999 (2018). https://doi.org/10.1002/celc.201801132
137. Yuan, X., Luo, Y.T., Zhang, B., et al.: Decoration of In nanoparticles on In_2S_3 nanosheets enables efficient electrochemical reduction of CO_2. Chem. Commun. **56**, 4212–4215 (2020). https://doi.org/10.1039/c9cc10078d
138. Lee, S., Park, G., Lee, J.: Importance of Ag-Cu biphasic boundaries for selective electrochemical reduction of CO_2 to ethanol.

ACS Catal. **7**, 8594–8604 (2017). https://doi.org/10.1021/acscatal.7b02822
139. Chen, Y.H., Kanan, M.W.: Tin oxide dependence of the CO_2 reduction efficiency on tin electrodes and enhanced activity for tin/tin oxide thin-film catalysts. J. Am. Chem. Soc. **134**, 1986–1989 (2012). https://doi.org/10.1021/ja2108799
140. Pander, J.E., III., Ren, D., Huang, Y., et al.: Understanding the heterogeneous electrocatalytic reduction of carbon dioxide on oxide-derived catalysts. ChemElectroChem **5**, 219–237 (2018). https://doi.org/10.1002/celc.201701100
141. Frese, K.W.: Electrochemical reduction of CO_2 at intentionally oxidized copper electrodes. J. Electrochem. Soc. **138**, 3338–3344 (1991). https://doi.org/10.1149/1.2085411
142. Ma, L.S., Hu, W.B., Mei, B.B., et al.: Covalent triazine framework confined copper catalysts for selective electrochemical CO_2 reduction: operando diagnosis of active sites. ACS Catal. **10**, 4534–4542 (2020). https://doi.org/10.1021/acscatal.0c00243
143. Matsumoto, H., Saito, K., Hasuo, M., et al.: Revived interest on yellow-exciton series in Cu_2C: an experimental aspect. Solid State Commun. **97**, 125–129 (1996). https://doi.org/10.1016/0038-1098(95)00601-X
144. Li, C.W., Kanan, M.W.: CO_2 reduction at low overpotential on Cu electrodes resulting from the reduction of thick Cu_2O films. J. Am. Chem. Soc. **134**, 7231–7234 (2012). https://doi.org/10.1021/ja3010978
145. Zhu, Q.G., Sun, X.F., Yang, D.X., et al.: Carbon dioxide electroreduction to C_2 products over copper-cuprous oxide derived from electrosynthesized copper complex. Nat. Commun. **10**, 1–11 (2019). https://doi.org/10.1038/s41467-019-11599-7
146. Ren, D., Deng, Y.L., Handoko, A.D., et al.: Selective electrochemical reduction of carbon dioxide to ethylene and ethanol on copper(I) oxide catalysts. ACS Catal. **5**, 2814–2821 (2015). https://doi.org/10.1021/cs502128q
147. Scholten, F., Sinev, I., Bernal, M., et al.: Plasma-modified dendritic Cu catalyst for CO_2 electroreduction. ACS Catal. **9**, 5496–5502 (2019). https://doi.org/10.1021/acscatal.9b00483
148. Engelbrecht, A., Hämmerle, M., Moos, R., et al.: Improvement of the selectivity of the electrochemical conversion of CO_2 to hydrocarbons using cupreous electrodes with in situ oxidation by oxygen. Electrochim. Acta **224**, 642–648 (2017). https://doi.org/10.1016/j.electacta.2016.12.059
149. Ma, S.C., Sadakiyo, M., Luo, R., et al.: One-step electrosynthesis of ethylene and ethanol from CO_2 in an alkaline electrolyzer. J. Power Sources **301**, 219–228 (2016). https://doi.org/10.1016/j.jpowsour.2015.09.124
150. Chen, C.S., Wan, J.H., Yeo, B.S.: Electrochemical reduction of carbon dioxide to ethane using nanostructured Cu_2O-derived copper catalyst and palladium(II) chloride. J. Phys. Chem. C **119**, 26875–26882 (2015). https://doi.org/10.1021/acs.jpcc.5b09144
151. Lee, S., Kim, D., Lee, J.: Electrocatalytic production of C_3–C_4 compounds by conversion of CO_2 on a chloride-induced bi-phasic Cu_2O-Cu catalyst. Angew. Chem. Int. Ed. **54**, 14701–14705 (2015). https://doi.org/10.1002/anie.201505730
152. Shang, L.M., Lv, X., Shen, H., et al.: Selective carbon dioxide electroreduction to ethylene and ethanol by core-shell copper/cuprous oxide. J. Colloid Interface Sci. **552**, 426–431 (2019). https://doi.org/10.1016/j.jcis.2019.05.073
153. Kibria, M.G., Dinh, C.T., Seifitokaldani, A., et al.: A surface reconstruction route to high productivity and selectivity in CO_2 electroreduction toward C_{2+} hydrocarbons. Adv. Mater. **30**, 1804867 (2018). https://doi.org/10.1002/adma.201804867
154. Mandal, L., Yang, K.R., Motapothula, M.R., et al.: Investigating the role of copper oxide in electrochemical CO_2 reduction in real time. ACS Appl. Mater. Interfaces **10**, 8574–8584 (2018). https://doi.org/10.1021/acsami.7b15418
155. Lum, Y., Ager, J.W.: Stability of residual oxides in oxide-derived copper catalysts for electrochemical CO_2 reduction investigated with ^{18}O labeling. Angew. Chem. Int. Ed. **57**, 551–554 (2018). https://doi.org/10.1002/anie.201710590
156. Fan, L., Xia, C., Yang, F.Q., et al.: Strategies in catalysts and electrolyzer design for electrochemical CO_2 reduction toward C_{2+} products. Sci. Adv. **6**, eaay3111 (2020). https://doi.org/10.1126/sciadv.aay3111
157. Xiao, H., Goddard, W.A., III., Cheng, T., et al.: Cu metal embedded in oxidized matrix catalyst to promote CO_2 activation and CO dimerization for electrochemical reduction of CO_2. PNAS **114**, 6685–6688 (2017). https://doi.org/10.1073/pnas.1702405114
158. Zhou, Y.S., Che, F.L., Liu, M., et al.: Dopant-induced electron localization drives CO_2 reduction to C_2 hydrocarbons. Nat. Chem. **10**, 974–980 (2018). https://doi.org/10.1038/s41557-018-0092-x
159. Zhang, L.Y., Yang, S., Lai, Y.K., et al.: In-situ synthesis of monodispersed Cu_xO heterostructure on porous carbon monolith for exceptional removal of gaseous Hg^0. Appl. Catal. B Environ. **265**, 118556 (2020). https://doi.org/10.1016/j.apcatb.2019.118556
160. Yang, S., Liu, Z.L., Yan, X., et al.: Catalytic oxidation of elemental mercury in coal-combustion flue gas over the $CuAlO_2$ catalyst. Energy Fuels **33**, 11380–11388 (2019). https://doi.org/10.1021/acs.energyfuels.9b02376
161. Mudiyanselage, K., Luo, S., Kim, H.Y., et al.: How to stabilize highly active Cu^+ cations in a mixed-oxide catalyst. Catal. Today **263**, 4–10 (2016). https://doi.org/10.1016/j.cattod.2015.08.025
162. Yin, Z.Y., Yu, C., Zhao, Z.L., et al.: Cu_3N nanocubes for selective electrochemical reduction of CO_2 to ethylene. Nano Lett. **19**, 8658–8663 (2019). https://doi.org/10.1021/acs.nanolett.9b03324
163. Huang, Q.L., Liu, H.M., An, W., et al.: Synergy of a metallic NiCo dimer anchored on a C_2N-graphene matrix promotes the electrochemical CO_2 reduction reaction. ACS Sustain. Chem. Eng. **7**, 19113–19121 (2019). https://doi.org/10.1021/acssuschemeng.9b05042
164. He, Y.H., Jiang, W.J., Zhang, Y., et al.: Pore-structure-directed CO_2 electroreduction to formate on SnO_2/C catalysts. J. Mater. Chem. A **7**, 18428–18433 (2019). https://doi.org/10.1039/c9ta05937g
165. Wang, Y., Zhou, J., Lv, W., et al.: Electrochemical reduction of CO_2 to formate catalyzed by electroplated tin coating on copper foam. Appl. Surf. Sci. **362**, 394–398 (2016). https://doi.org/10.1016/j.apsusc.2015.11.255
166. Yang, Y., Zhang, Y., Hu, J.S., et al.: Progress in the mechanisms and materials for CO_2 electroreduction toward C_{2+} products. Acta Phys. Chim. Sin. **36**, 1906085 (2020). https://doi.org/10.3866/PKU.WHXB201906085
167. Grosse, P., Gao, D.F., Scholten, F., et al.: Dynamic changes in the structure, chemical state and catalytic selectivity of Cu nanocubes during CO_2 electroreduction: size and support effects. Angew. Chem. Int. Ed. **57**, 6192–6197 (2018). https://doi.org/10.1002/anie.201802083
168. Geioushy, R.A., Khaled, M.M., Hakeem, A.S., et al.: High efficiency graphene/Cu_2O electrode for the electrochemical

reduction of carbon dioxide to ethanol. J. Electroanal. Chem. **785**, 138–143 (2017). https://doi.org/10.1016/j.jelechem.2016.12.029
169. Song, Y., Peng, R., Hensley, D.K., et al.: High-selectivity electrochemical conversion of CO_2 to ethanol using a copper nanoparticle/N-doped graphene electrode. ChemistrySelect **1**, 6055–6061 (2016). https://doi.org/10.1002/slct.201601169
170. Lim, D.H., Jo, J.H., Shin, D.Y., et al.: Carbon dioxide conversion into hydrocarbon fuels on defective graphene-supported Cu nanoparticles from first principles. Nanoscale **6**, 5087–5092 (2014). https://doi.org/10.1039/c3nr06539a
171. Li, Q., Zhu, W.L., Fu, J.J., et al.: Controlled assembly of Cu nanoparticles on pyridinic-N rich graphene for electrochemical reduction of CO_2 to ethylene. Nano Energy **24**, 1–9 (2016). https://doi.org/10.1016/j.nanoen.2016.03.024
172. Lv, K., Fan, Y.C., Zhu, Y., et al.: Elastic Ag-anchored N-doped graphene/carbon foam for the selective electrochemical reduction of carbon dioxide to ethanol. J. Mater. Chem. A **6**, 5025–5031 (2018). https://doi.org/10.1039/c7ta10802h
173. Huo, Y.J., Peng, X.Y., Liu, X.J., et al.: High selectivity toward C_2H_4 production over Cu particles supported by butterfly-wing-derived carbon frameworks. ACS Appl. Mater. Interfaces **10**, 12618–12625 (2018). https://doi.org/10.1021/acsami.7b19423
174. Daiyan, R., Lovell, E.C., Bedford, N.M., et al.: Modulating activity through defect engineering of tin oxides for electrochemical CO_2 reduction. Adv. Sci. **6**, 1900678–1900687 (2019). https://doi.org/10.1002/advs.201900678
175. Zhang, Y.F., Liu, J.J., Wei, Z.X., et al.: Single-layer oxygen deficiency δ-MnO_2 for electrochemical CO_2 reduction. J. Electrochem. **25**, 477–485 (2019). https://doi.org/10.13208/j.electrochem.180945
176. Dong, H., Zhang, L., Li, L.L., et al.: Abundant Ce^{3+} ions in Au-CeO_x nanosheets to enhance CO_2 electroreduction performance. Small **15**, 1900289 (2019). https://doi.org/10.1002/smll.201900289
177. Cui, X.Q., Pan, Z.Y., Zhang, L.J., et al.: CO_2 reduction: selective etching of nitrogen-doped carbon by steam for enhanced electrochemical CO_2 reduction. Adv. Energy Mater. **7**, 1701456 (2017). https://doi.org/10.1002/aenm.201770126
178. Michalsky, R., Zhang, Y.J., Medford, A.J., et al.: Departures from the adsorption energy scaling relations for metal carbide catalysts. J. Phys. Chem. C **118**, 13026–13034 (2014). https://doi.org/10.1021/jp503756g
179. Wang, Z., Yang, G., Zhang, Z., et al.: Selectivity on etching: creation of high-energy facets on copper nanocrystals for CO_2 electrochemical reduction. ACS Nano **10**, 4559–4564 (2016). https://doi.org/10.1021/acsnano.6b00602
180. Xie, M.S., Xia, B.Y., Li, Y.W., et al.: Amino acid modified copper electrodes for the enhanced selective electroreduction of carbon dioxide towards hydrocarbons. Energy Environ. Sci. **9**, 1687–1695 (2016). https://doi.org/10.1039/c5ee03694a
181. Francis, S.A., Velazquez, J.M., Ferrer, I.M., et al.: Reduction of aqueous CO_2 to 1-propanol at MoS_2 electrodes. Chem. Mater. **30**, 4902–4908 (2018). https://doi.org/10.1021/acs.chemmater.7b04428
182. Calvinho, K.U.D., Laursen, A.B., Yap, K.M.K., et al.: Selective CO_2 reduction to C_3 and C_4 oxyhydrocarbons on nickel phosphides at overpotentials as low as 10 mV. Energy Environ. Sci. **11**, 2550–2559 (2018). https://doi.org/10.1039/c8ee00936h
183. Gao, D., Zegkinoglou, I., Divins, N.J., et al.: Plasma-activated copper nanocube catalysts for efficient carbon dioxide electroreduction to hydrocarbons and alcohols. ACS Nano **11**, 4825–4831 (2017). https://doi.org/10.1021/acsnano.7b01257
184. Fields, M., Hong, X., Nørskov, J.K., et al.: Role of subsurface oxygen on Cu surfaces for CO_2 electrochemical reduction. J. Phys. Chem. C **122**, 16209–16215 (2018). https://doi.org/10.1021/acs.jpcc.8b04983
185. Garza, A.J., Bell, A.T., Head-Gordon, M.: Is subsurface oxygen necessary for the electrochemical reduction of CO_2 on copper? J. Phys. Chem. Lett. **9**, 601–606 (2018). https://doi.org/10.1021/acs.jpclett.7b03180

Fangfang Chang is a lecturer at School of Chemistry and Chemical Engineering at Henan Normal University. She received her Ph.D. degree in Chemistry from Hunan University in 2017. Her research interests include nanoscale catalyst synthesis, characterization and application in clean energy conversion technologies such as fuel cells, electrochemical reduction of CO_2.

Meiling Xiao received her Bachelor's degree from Nanjing Normal University, China, in 2011 and Ph.D. degree in Physical Chemistry from Changchun Institute of Applied Chemistry, Chinses Academy of Sciences in 2016. Currently, she works as a postdoctoral research fellow in the University of Waterloo, now her research interests focus on the exploration of earth-abundant materials to replace noble metal materials for electrocatalytic process and the understanding of electrocatalysis mechanism on these novel electrocatalysts.

Ruifang Miao received her Master's degree in 2021 from Henan Normal University. Her research interests focus on the rational design of functional nanomaterials and their application in electrocatalytic carbon dioxide reduction.

Yongpeng Liu is currently a Master degree candidate at Henan Normal University. She received her Bachelor's degree in Chemistry and Chemical Engineering at the Pingdingshan University in 2016. Her research interests include the rational design of functional nanomaterials and their applications in electrocatalysis and fuel cells.

Mengyun Ren received her Master's degree in 2021 from Henan Normal University. Her research interests include design, synthesis and characterization of robust, active and low-cost nanoparticle catalysts for reactions related to clean energy conversion technologies.

Zhichao Jia is a Ph.D. candidate at Henan Normal University. His research field involves the rational design of functional nanomaterials and their applications in biotransformation, electrocatalytic CO_2 reduction and oxygen evolution reaction.

Dandan Han is currently a Master candidate at Henan Normal University. She received her Bachelor's degree in Chemistry at Xinyang College in 2019. Her research interests include the reasonable design of catalytic materials for electrocatalysis of carbon dioxide and study on the mechanism of influencing the catalytic products.

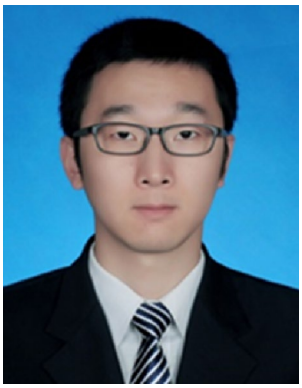

Yang Yuan received his Ph.D. degree from Jilin University in 2019 under the supervision of Prof. Yunling Liu. During his doctoral studies, he researched on design and synthesis of novel metal-organic frameworks for catalysis. Now, he is a Postdoctoral Fellow in the group of Prof. Lin Yang in Henan normal university. His research interests mainly focus on rational design of nanoscale carbon-based non-noble metal catalysts, especially the MOFs-derived metal single-atomic (SA) catalysts, and their application in oxygen reduction toward fuel cells.

Zhengyu Bai is a professor at School of Chemistry and Chemical Engineering at Henan Normal University. She received her Ph.D. degree in 2010 from Henan Normal University. She received the Distinguished Young Investigator Awards at the 4th International Conference on Electrochemical Energy Science and Technology 2018 (EEST 2018). Her research is focused on new green energy nanomaterials, such as nanostructured electrocatalysts for fuel cell and metal-air batteries. Dr. Bai has published over 80 peer-reviewed journal articles. She is also listed as an inventor on 25 national patents, with 8 patents licensed in China.

Lin Yang is a professor at School of Chemistry and Chemical Engineering at Henan Normal University. He received his Ph.D. degree from Lanzhou Institute of Chemical Physics, Chinese Academy of Sciences in 2003. He is a member of International Academy of Electrochemical Energy Science (IAOEES), the leader of national "Green Chemistry and Power Source Materials" discipline innovation base and the vice director of Key Laboratory of Green Chemical Media and Reactions from Ministry of Education. His research is focused on biological fuel cell, fuel cell and green energy storage nanomaterials. He has published more than 200 peer reviewed papers.